

1 **Impacts of condensable particulate matter on atmospheric organic aerosols and fine**
2 **particulate matter (PM_{2.5}) in China**

3
4 Mengying Li¹, Shaocai Yu¹⁺, Xue Chen¹, Zhen Li¹, Yibo Zhang¹, Zhe Song¹, Weiping Liu¹, Pengfei
5 Li²⁺, Xiaoye Zhang^{1,3}, Meigen Zhang^{4,5,6}, Yele Sun^{4,5}, Zirui Liu^{4,5}, Caiping Sun⁷, Jingkun Jiang^{8,9},
6 Shuxiao Wang⁸, Benjamin N. Murphy¹⁰, Kiran Alapaty¹⁰, Rohit Mathur¹⁰, Daniel Rosenfeld¹¹, and John
7 H. Seinfeld¹²
8

9 ¹Research Center for Air Pollution and Health; Key Laboratory of Environmental Remediation and
10 Ecological Health, Ministry of Education, College of Environment and Resource Sciences, Zhejiang
11 University, Hangzhou, Zhejiang 310058, P.R. China

12 ²College of Science and Technology, Hebei Agricultural University, Baoding, Hebei 071000, P.R. China

13 ³Chinese Academy of Meteorological Sciences, China Meteorological Administration, Beijing 100081,
14 China.

15 ⁴State Key Laboratory of Atmospheric Boundary Layer Physics and Atmospheric Chemistry (LAPC),
16 Institute of Atmospheric Physics (IAP), Chinese Academy of Sciences (CAS), Beijing 100029, China

17 ⁵University of Chinese Academy of Sciences, Beijing 100049, China

18 ⁶Center for Excellence in Urban Atmospheric Environment, Institute of Urban Environment, Chinese
19 Academy of Sciences, Xiamen, China

20 ⁷Chinese Research Academy of Environmental Sciences, Beijing 100012, China

21 ⁸State Key Joint Laboratory of Environment Simulation and Pollution Control, School of Environment,
22 Tsinghua University, Beijing 100084, China

23 ⁹State Environmental Protection Key Laboratory of Sources and Control of Air Pollution Complex,
24 Beijing 100084, China

25 ¹⁰Center for Environmental Measurement and Modeling, U.S. Environmental Protection Agency,
26 Research Triangle Park, NC 27711, USA

27 ¹¹Institute of Earth Sciences, The Hebrew University of Jerusalem, Jerusalem, Israel

28 ¹²Division of Chemistry and Chemical Engineering, California Institute of Technology, Pasadena, CA
29 91125, USA.

30
31
32 ⁺*Correspondence to:* Shaocai Yu (shaocaiyu@zju.edu.cn); Pengfei Li (lpf_zju@163.com)

33
34 **To be submitted to**

35 **Atmospheric Chemistry and Physics**

36 **Abstract**

37 Condensable particulate matter (CPM) emitted from stationary combustion and mobile sources
38 exhibits high emissions and a large proportion of organic components. However, CPM is not generally
39 measured when conducting emission surveys of PM in most countries, including China. Consequently,
40 previous emission inventories have not included emission rates for CPM. Here we construct an emission
41 inventory of CPM in China with a focus on organic aerosols (OA) based on collected CPM emission
42 information. Results show that OA emissions are enhanced twofold after the inclusion of CPM in a new
43 China inventory for the years 2014 and 2017. Considering organic CPM emissions and model
44 representations of secondary OA (SOA) formation from CPM, here a series of sensitivity cases have been
45 simulated using the three-dimensional Community Multiscale Air Quality (CMAQ) model to estimate the
46 contributions of CPM emissions to atmospheric OA and fine PM (PM_{2.5}) concentrations in China.
47 Compared with observations during a haze episode from October 14 to November 14, 2014, at a Beijing
48 site, estimates of temporal average primary OA (POA) and SOA concentrations are greatly improved after
49 including the CPM effects. These scenarios demonstrated the significant contributions of CPM emissions
50 from stationary combustion and mobile sources to POA (51 ~ 85%), SOA (42 ~ 58%), and total OA
51 concentrations (45 ~ 75%). Furthermore, contributions of CPM emissions to total OA concentrations were
52 demonstrated over the major 2+26 cities of Beijing-Tianjin-Hebei region (BTH2+26 cities) in December
53 2018, with average contributions up to 49%, 53%, 54%, and 50% for Handan, Shijiazhuang, Xingtai, and
54 Dezhou, respectively. Correspondingly, the inclusion of CPM emissions also narrowed the gap between
55 simulated and observed PM_{2.5} concentrations over the BTH2+26 cities. These results improve the
56 simulation performance of atmospheric OA and PM_{2.5}, and may provide important implications for the
57 sources of OA.

58

59

60

61

62

63

64

65

66

67 **1 Introduction**

68 Atmospheric fine particulate matter (PM_{2.5}, particulate matter with aerodynamic diameter not
69 exceeding 2.5 μm) is a serious and recurring air quality problem. Although the annual average
70 concentration of PM_{2.5} in China has declined in recent years, it still exceeds standards promulgated by the
71 World Health Organization (WHO) Air Quality Guidelines (Lin et al., 2018). Heavy haze episodes occur
72 frequently in winter, especially for the eastern regions in China (Li et al., 2015; Chen et al., 2019; Li et
73 al., 2017a). Despite large reductions in primary emissions during the COVID-19 lockdown, several
74 periods of heavy haze continued to occur in eastern China (Huang et al., 2021; Wang et al., 2020c, 2021).
75 Organic aerosols (OA) contribute a large fraction to the PM_{2.5} worldwide, ranging from 20% to 90%
76 (Carlton et al., 2009; Kanakidou et al., 2005) with a negative radiative forcing and adverse impacts on a
77 negative impact on radiative climate forcing, air quality and human health (Gehring et al., 2013; Pope et
78 al., 2002). POA comes from a variety of sources, including fossil fuels and biomass burning. SOA is
79 generated through photochemical oxidation of volatile organic compounds (VOCs) followed by gas-
80 particle partitioning of low-volatility organic compounds into the aerosol phase (Fuzzi et al., 2006; Kroll
81 and Seinfeld, 2008) Currently, the significant contributions of OA to PM_{2.5} and SOA to OA have been
82 demonstrated in many observational results (He et al., 2020; Veld et al., 2021; Zhang et al., 2017). For
83 example, Huang et al. (2015) explored the role of OA in PM_{2.5} during a severe haze episode in Beijing,
84 Shanghai, Xi'an and Guangzhou, showing the substantial contribution of OA to PM_{2.5} (30~50%) and SOA
85 accounted for 30~77% of OA. Sun et al. (2015) showed that OA constituted up to 65% of submicron
86 aerosols during winter in Beijing, with 38% being SOA.

87 With respect to chemical schemes of SOA formations, a two-product model (Odum et al., 1996) was
88 first proposed based on absorptive partitioning theory (Pankow, 1994) and chamber data. To address the
89 underestimation of the early two-product model, the volatility basis set (VBS) framework was developed
90 (Donahue et al., 2006). In this VBS scheme, semi-volatile and intermediate volatility precursors (S/IVOCs)
91 were classified by their volatilities based on the absorptive partitioning theory (Robinson et al., 2007). A
92 large portion of SVOCs are emitted as POA and then evaporate at ambient conditions due to gas-particle
93 partitioning, while the IVOCs species exist in the form of organic vapor under many atmospheric
94 conditions in the absence of photochemical reactions (Shrivastava et al., 2011). Currently, the VBS
95 mechanism has been incorporated into many global and regional scale models (Lane et al., 2008; Murphy
96 and Pandis, 2009; Shrivastava et al., 2008; Han et al., 2016). The two-dimensional (2-D) VBS scheme
97 was put forward to improve the accuracy of fragmentation processes and OA oxidations (Donahue et al.,

98 2011; Zhao et al., 2016). Despite advances in SOA formation mechanisms, a gap exists between observed
99 and modeled results due to uncertainties in parameterization of SOA yields, lack of localized parameters
100 ~~inapplicability of parameter localizations caused by regional and sectoral differences~~ and incomplete
101 information on emission rates and properties of SOA precursors. Recent studies have begun to focus on
102 important effects of emissions, including traditional precursors (VOCs) and low-volatility precursors
103 (S/IVOCs). For example, Zhao et al. (2017) found that IVOC of 1.5–30 times POA emissions contributed
104 largely to OA concentrations over the BTH region. Wu et al. (2019) constructed an inventory of S/IVOCs
105 for the Pearl River Delta (PRD) region in China and conducted a simulation using the WRF-Chem model
106 leading to an increase of 161% in SOA predictions. Emissions of S/IVOCs from mobile sources and
107 IVOCs from volatile chemical products were also parameterized in models to represent SOA formation
108 (Jathar et al., 2017; Lu et al., 2020; Pennington et al., 2021). Although the significant role of potential
109 emission sources in OA formation has been demonstrated, underestimation of SOA by current air quality
110 models has not been totally resolved. Stationary combustion sources are one of the major emission sources
111 of PM_{2.5}, including power plants and factories. Sampling temperatures and dilution rates are key factors
112 for accurate measurements of organic matter (Morino et al., 2018). The total primary PM emitted from
113 stationary sources is composed of filterable PM (FPM) and condensable PM (CPM). FPM exists in liquid
114 or solid phases, while CPM is in gas phase in flue (Corio and Sherwell, 2000; Feng et al., 2018). CPM is
115 defined by the U.S. Environmental Protection Agency (EPA, 2017) as particles which are gaseous at flue
116 gas temperature but condense or react in the ambient air to form solid or liquid PM through dilution and
117 cooling immediately after discharge. With ultralow emission standards implemented by coal-fired power
118 plants (<10 mg/Nm³) since 2014, FPM emissions have been substantially reduced (even below 5 mg/Nm³)
119 (Tang et al., 2019), making the remaining emissions of CPM an important issue. The Ministry of Science
120 and Technology of China issued a national key research and development project on the causes and
121 controls of air pollution in 2016, which mentioned key technologies for controlling CPM emissions
122 ([http://www.acca21.org.cn/zdy_cms/siteResources/DisasterReduction/resources/otherfiles/
20160425/f15345793.pdf](http://www.acca21.org.cn/zdy_cms/siteResources/DisasterReduction/resources/otherfiles/20160425/f15345793.pdf)). The current measurement studies about emission characteristics and chemical
123 composition of CPM exhibited non-negligible emissions. For example, Yang et al. (2014, 2018a, 2018b)
124 conducted investigations for different types of industrial boilers and power plants, and concluded that
125 CPM constituted 25.7~96.5% of PM_{2.5}. For an ultralow-emission coal-fired power plant, Li et al. (2017b)
126 reported that the emission concentrations of CPM accounted for 83% of the PM_{2.5}. Wang et al. (2018)
127 calculated the average emission factors of CPM from two stacks in a waste incineration power plant to
128

129 be 0.201 and 0.178 g/kg, which were 22.0 and 31.2 times higher than the corresponding those of FPM,
130 respectively. Wu et al. (2020) found that FPM emissions from four typical coal-fired power plants met
131 Chinese ultra-low emission standards, while CPM showed high levels (even above 10 mg/Nm³). CPM
132 includes organic and inorganic components, known as organic CPM and inorganic CPM, respectively.
133 The contributions of organic fractions varied from 13.6% to 80.5%, depending on different fuel types,
134 test methods and operating conditions (Lu et al., 2019; Song et al., 2020; Yang et al., 2021, 2018b). Many
135 studies confirmed that more than 50% of organic composition were measured in CPM (Li et al., 2017c,
136 2017d; Song et al., 2020; Wu et al., 2020), revealing that organic matter comprising a large proportion in
137 CPM needed to be taken into account. These above studies provided valuable basic information of CPM
138 emission characteristics for data references in this study, as summarized in Table S3. It is likely that the
139 inorganic fractions of CPM make a contribution to the water-soluble ions in PM_{2.5}, and organic
140 components contribute to the organic matter in PM_{2.5}. In addition, large amounts of low volatile organic
141 compounds in CPM can be important precursors for SOA formation.

142 Current measurement methods for PM in stationary exhaust sources in China (GB/T 16157-1996)
143 have not involved the collections of CPM; and the chemical composition of collected PM was quite
144 different from that actually released into the atmosphere (Hu et al., 2016). The emission inventory
145 constructed based on emission surveys did not include the CPM emissions. So it is important to introduce
146 CPM emissions to the current emission inventory. For example, a European study improved OA
147 simulations by including the CPM emissions from residential wood combustion sources (Van Der Gon et
148 al., 2015). Morino et al. (2018) revised the emission inventory by the consideration of CPM in Japan and
149 showed that the OA emission rates were up to seven times the previous ones and CPM contributed largely
150 to atmospheric OA concentrations. A shortcoming of that study was that it did not separate the effects of
151 CPM emissions on POA and SOA concentrations. Moreover, studies still lack quantification of emissions
152 of CPM released by stationary combustion sources in China.

153 In this study, we use the available CPM emission information to construct an emission inventory of
154 CPM from stationary combustion and mobile sources in China (with a focus on OA) and conducted 15
155 sensitivity simulations to explore the contributions of CPM emissions to atmospheric OA and PM_{2.5}
156 concentrations during the winter haze episodes over China. This quantitative study about organic CPM
157 emissions and the roles of CPM in the OA formation emphasizes the importance of constraining CPM
158 emissions from stationary combustion and mobile sources.

159

2 Materials and methods

2.1 Estimations of CPM emissions

Table 1 explicitly states the definitions of some acronyms for better understanding. We collected available emission measurement data of CPM based on published literatures. Totally, CPM emission data from 52 stationary combustion sources were acquired (Table S3). The emission sectors for these data included coal-fired power plants, waste incineration power plants, industrial coal boilers, heavy oil boilers, wood boilers, natural gas boilers, diesel boilers, iron and steel plants, and incinerators. Emissions of CPM depend on many factors including source categories, fuel types, sampling flue gas temperature, and air pollution control devices (Feng et al., 2021). Also, different measurement methods produced different results of CPM emissions (Wang et al., 2020a). Recently, cooling and dilution methods have been applied to monitor CPM concentrations. CPM contained organic and inorganic fractions, but this study only concentrated on organic CPM emissions. The emission rate of OA in CPM was estimated as follows in Eq. (1) and (2) (Morino et al., 2018):

$$E_{OM}(CPM) = \sum A \times EF_{OM}(CPM) = \sum A \times EF_{PM_{2.5}}(FPM) \times \frac{EF_{OM}(CPM)}{EF_{PM_{2.5}}(FPM)} \quad (1)$$

$$E_{OM}(CPM) = \sum E_{PM_{2.5}}(FPM) \times \frac{C_{OM}(CPM)}{C_{PM_{2.5}}(FPM)} \quad (2)$$

$$E_{OM_{si}}(CPM) = E_{OM}(CPM) \times \frac{E_{OM_{si}}(CPM)}{E_{OM}(CPM)} = E_{OM}(CPM) \times \frac{C_{OM_{si}}(CPM)}{C_{OM}(CPM)} \quad (3)$$

Where $E_{OMA}(CPM)$ is the emission rate of organic matter in CPM; $EF_{OMA}(CPM)$ is the emission factor of organic matter in CPM; $E_{PM_{2.5}}(FPM)$ is the emission rate of $FPM_{2.5}$; $EF_{PM_{2.5}}(FPM)$ is the emission factor of $FPM_{2.5}$; A denotes the activity level; $C_{OMA}(CPM)$ is the concentration of organic matter detected in CPM; and $C_{PM_{2.5}}(FPM)$ is the detected concentration of $FPM_{2.5}$. A and $EF_{PM_{2.5}}(FPM)$ in Eq. (1) were combined to calculate $E_{PM_{2.5}}(FPM)$ in Eq. (2), acquired from $PM_{2.5}$ emission rates in the emission inventory of baseline year. Among these parameters, $C_{OMA}(CPM)$ and $C_{PM_{2.5}}(FPM)$ were derived from the collected emission survey data at the above stationary combustion sources. The ratios of $C_{OMA}(CPM)$ to $C_{OMA}(FPM)$ can-should be used to estimate $E_{OMA}(CPM)$, but due to the limited data and very low values of $C_{OMA}(FPM)$ at stationary sources, $C_{PM_{2.5}}(FPM)$ was used instead of $C_{OMA}(FPM)$. The ratios of $E_{OMA}(CPM)$ to $E_{PM_{2.5}}(FPM)$ and $EF_{OMA}(CPM)$ to $EF_{PM_{2.5}}(FPM)$ should be equal to the ratios of $C_{OMA}(CPM)$ to $C_{PM_{2.5}}(FPM)$ at the same dilution ratio in the emission surveys, as summarized in Table 1. Table 2 summarizes the emission ratios of $E_{OM}(CPM)$ to $E_{PM_{2.5}}(FPM)$ for these stationary combustion sources. In this estimate, these emission ratios collected from the best available data from the stationary

189 ~~sources~~ were applied to represent the stationary combustion sources in the current emission inventory.

190 In addition, the component information of organic CPM is important to model the participation of
191 organic CPM in atmospheric chemical reactions. A and $EF_{PM_{2.5}}(FPM)$ in Eq. (1) were combined to get
192 $E_{PM_{2.5}}(FPM)$ in Eq. (2), acquired from $PM_{2.5}$ emission rates in the emission inventory of baseline year.

193 The organic CPM mainly contains alkanes (with C_{10} - C_{30} being the major n-alkanes), esters, and
194 polycyclic aromatic hydrocarbons (PAHs) (Li et al., 2017c, d; Song et al., 2020; Zheng et al., 2018).

195 Based on the relationship between carbon number of n-alkanes and saturation concentrations (C^*)
196 following Lu et al. (2018), it is reasonable to speculate that organic CPM is composed of organic matter

197 which is semi-volatile (SVOCs, $10^0 \leq C^* \leq 10^3 \mu\text{g m}^{-3}$) or has intermediate volatility (IVOCs, $10^3 < C^* \leq$
198 $10^6 \mu\text{g m}^{-3}$), combined as OM_{si} (CPM).~~organic CPM is composed of organic matter which has low~~

199 ~~volatility (LVOC, $10^{-3} < C^* < 10^0$), semi-volatile (SVOC, $10^0 < C^* < 10^3$), or has intermediate volatility~~
200 ~~(IVOC, $10^3 < C^* < 10^6$), combined as OM_{lsi} (CPM).~~ Since the volatility characteristics of organic CPM from

201 these stationary combustion sources have not been accurately determined in relevant measurement studies,
202 the emissions of ~~OM_{si} (CPM)~~ ~~OM_{lsi} (CPM)~~ were scaled to emissions of ΘAOM (CPM) in this estimate as

203 shown in Eq. (3), that is, the total emissions of OM (CPM) were distributed in different volatility bins.
204 $E_{OM_{si}}$ (CPM) ~~$E_{OM_{lsi}}$ (CPM)~~ denotes the emission rate of ~~OM_{si}~~ ~~OM_{lsi}~~ in CPM; $C_{OM_{si}}$ (CPM) denotes the

205 concentration of OM_{si} in CPM. ~~$C_{OM_{lsi}}$ (CPM) is the concentration of OM_{lsi} in CPM.~~ The specific partition
206 coefficients for different volatility bins in the model will be discussed in the following Sect. 2.3. In

207 addition to stationary sources, mobile sources also generate certain emissions of CPM. Due to the lack of
208 CPM emission data from on-road and off-road vehicles, we increased $OM\Theta A$ emission rates of the

209 transportation sector (TR) by 30% to consider the contributions of CPM from these mobile sources,
210 following Morino et al. (2018) and Lu et al. (2020).

212 2.2 The model configuration

213 The three-dimensional Community Multiscale Air Quality (CMAQ, v5.3.2) model developed by the
214 U.S. Environmental Protection Agency was used to simulate spatiotemporal distributions of chemical
215 species. The detailed model configuration can ~~be referred~~refer to Appel et al. (2021) and Yu et al. (2014).

216 The gas-phase chemical mechanism was based on the Carbon Bond Mechanism 6 (CB6) scheme. The
217 aerosol module was based on the seventh-generation aerosol module of CMAQ (AERO7). The

218 CMAQv5.0.2-VBS version with AERO6 coupled with a VBS module (AERO6VBS) was used for
219 comparison. Compared to the SOA formation in AERO6 in the CMAQv5.2, the AERO7 module includes

220 improvements: enhanced consistency of the SOA formation pathways between chemical mechanisms
221 based on CB and SAPRC, updated photooxidized monoterpene SOA yields (Xu et al., 2018), added
222 uptake of water by hydrophilic organics (Pye et al., 2017), consumption of inorganic sulfate when forming
223 isoprene epoxydiol organic sulfate (Pye et al., 2013), and replacement of the Odum two-product model
224 with a VBS framework to parameterize SOA formation (Qin et al., 2021; Appel et al., 2021). Both
225 AERO6VBS and AERO7 contained five classes of organic matter with one class being nonvolatile and
226 the other four classes being semi-volatile with effective saturation concentrations of 1, 10, 100, and 1000
227 $\mu\text{g m}^{-3}$. Each of these volatility bins was assigned to the CMAQ species of LVPO1, SVPO1, SVPO2,
228 SVPO3 and IVPO1, respectively. The emissions of unspiciated IVOC were set equal to 1.5 times the
229 POA emissions in AERO6VBS and 6.579 times in AERO7 by default (Table 3). The high scale factor of
230 6.579 in AERO7 was set to consider missing pathways for the SOA formation from combustion sources
231 including the IVOC oxidation (Murphy et al., 2017; Murphy et al., 2021), and it was primarily
232 parameterized in Los Angeles where vehicle emissions are a principal source (Hayes et al., 2015). This
233 parameter setting may not be suitable for fire and wood-burning sources, thus the scale factor was zeroed
234 out for these sources in this study, as stated in the release of CMAQv5.3.2 and might have accounted for
235 the CPM contributions. In addition, the ratios of C_{SIVOCs} to C_{OA} can be dependent on C_{OA} under stack
236 conditions, which were generally above $3000 \mu\text{g m}^{-3}$ in CPM according to the emission surveys.
237 Considering high OA concentrations, we revised the scale factor of IVOC to 1.5 (same as that in
238 AERO6VBS) in the AERO7_adj case which was regarded as the base case. Meteorological fields were
239 predicted by the Weather Research and Forecasting (WRF) model version 3.7. The physical schemes of
240 WRF were the same as those in Wu et al. (2018) and Zhang et al. (2021). Meteorological initial and
241 boundary conditions were provided by the National Center for Environmental Prediction (NCEP) final
242 analysis dataset with the spatial resolution of $1^\circ \times 1^\circ$ and temporal resolution of 6 h. The first several days
243 were used for model spin-up, varied for different pollution periods as described in Sect. 2.4. The gridded
244 anthropogenic emission data for 2014 and 2017 were derived from Emission Inventory of Air Benefit and
245 Cost and Attainment Assessment System (EI-ABaCAS) developed by Tsinghua University (Dong et al.,
246 2020; Zheng et al., 2019). It contained primary species such as $\text{PM}_{2.5}$, SO_2 , NO_x , CO, NMVOCs, NH_3 ,
247 BC, and OC from nine anthropogenic sectors (i.e., agriculture, power plant, industry process, industry
248 combustion, steel, cement, residential, transport, and open burning). Biogenic source emissions were
249 calculated by on-line Biogenic Emission Inventory System version 3.14 (BEISv3.14) model (Carlton and
250 Baker, 2011). Dust emissions were calculated by an on-line windblown dust scheme (Choi and Fernando,

2008). Our study period in 2014 occurred before and during the Asia-Pacific Economic Cooperation (APEC) summit held in Beijing (November 5–11, 2014). During the period of pre-APEC (October 28–November 2) and full-APEC (November 3–11), some pollution control measures were gradually implemented in Beijing and its surrounding areas. Based on the observed reductions in the concentrations of PM_{2.5}, SO₂, NO₂, NO, and CO during APEC in Beijing and its surrounding cities (Li et al., 2017e, 2019; Wen et al., 2016), and 28% contribution of the emission control measures to the reduction of PM_{2.5} concentrations (Liang et al., 2017), thus the approximate emission reduction of 30% was conducted during the above time period for the region of ~~Thus we conducted emission reduction by 30% during the above time period for~~ two municipalities (Beijing and Tianjin), four provinces (Hebei, Shanxi, Henan, and Shandong), and Inner Mongolia Autonomous Region ~~(Li et al., 2017e, 2019)~~. The simulation domain covered mainland China by a 395 × 345 grid with the horizontal grid resolution of 12 km (Fig. 1). There were 29 vertical layers in σ_z coordinate system reaching the upper pressure (100 hPa) with 20 layers located in the lowest 3 km to resolve the planetary boundary layer.

2.3 Design of sensitivity simulation cases

According to the emission parameters summarized in Table 1, we carried out bootstrapping and Monte Carlo simulations to obtain the mean and uncertainty ranges of $E_{\text{OMA}}(\text{CPM})/E_{\text{PM}_{2.5}}(\text{FPM})$ for stationary combustion sources including power plant (PP), industry combustion (IN), steel (IR) (see Table [32](#)). First, the optimal probabilistic distributions and uncertainty ranges were determined for each source category. Then the statistical bootstrap simulation was applied to calculate the mean and 95% confidence interval of emission ratios for each source category. Finally, the uncertainties of these parameters were propagated to calculate the total uncertainty of emission by running Monte Carlo simulations for 10,000 times. Notably, the estimated uncertainties were only related to variabilities in the ratio of $E_{\text{OM}}(\text{CPM})$ to $E_{\text{PM}_{2.5}}(\text{FPM})$, but did not necessarily represent the overall uncertainties of organic CPM emissions. On this basis, a series of sensitivity cases including low, medium, and high emission ratios were designed to explore the contributions of organic CPM emissions to OA concentrations and quantify uncertainty ranges of CPM effects on OA (see Table [43](#)).

Here, to explore the contributions of organic CPM emissions to atmospheric OA and PM_{2.5} concentrations, the estimated emissions of organic CPM were added into the CMAQ model as an individual source, separated from other emission sources. For the base scenarios, the simulations were performed with the input of the previous emission inventory without the newly constructed organic CPM

emissions ~~in the AERO6VBS, AERO7_def and AERO7_adj cases.~~ Considering that organic FPM from stationary combustion and mobile sources mainly contained low volatile matter, so all of these emissions should be assigned to the CMAQ species of LVPO1 and other volatility bins should be assigned a scale factor of 0, and the rests were kept at the default settings in the model. ~~Except the revision of scale factor of IVOC in AERO7_adj case, the rests were kept at the default settings in the model.~~ ~~On the other hand,~~ In addition, different volatility distributions could be chosen for different emission sources, but this was not our study focus and did not interfere with the results of CPM contributions. For the ~~other~~ cases including CPM emissions from stationary combustion and mobile sources, the emissions of organic CPM were mapped to surrogate species ~~of for~~ different volatility bins (LVPO1, SVPO1, SVPO2, SVPO3, and IVPO1) in the CMAQ model for representing the SOA formation from CPM. These mixed species underwent gas-particle partitioning and multi-generational gas-phase photochemical oxidation of organic vapors by OH radicals to generate successively lower volatility and more-oxygenated species, and then produced SOA. Due to the unavailable volatility distribution information of $OM_{si}(CPM)$ ~~$OM_{si}(CPM)$~~ , different scaling factors of volatility bins were employed under each emission scenario to discuss the uncertainties of CPM effects. In this study, we tested two kinds of scaling factors for the five volatility bins ~~of SVOC~~: fac1 (0.09, 0.09, 0.14, 0.18, 0.5) (Grieshop et al., 2009), fac2 (0.40, 0.26, 0.40, 0.51, 1.43) (Shrivastava et al., 2011). As mentioned in Sect. 2.1, organic CPM was composed of organic matter which was semi-volatile or had intermediate volatility, thus the first bin which represents nonvolatile organic matter should be set to zero. Here, the original partition coefficient of the first bin was added to the following bin, so the fac1 (0, 0.18, 0.14, 0.18, 0.5) and fac2 (0, 0.66, 0.40, 0.51, 1.43) were applied in the sensitivity simulation cases. The fac2 estimated total SVOC emissions as 3 times POA emissions to consider missing $OM_{si}(CPM)$ emissions. ~~Although the high coefficient settings may lead to overestimation of the simulations, it was still applied to discuss the sensitivity of modeling results to different volatility distributions.~~ ~~Then the fac3 (0.245, 0.175, 0.27, 0.345, 0.965) which is the average of fac1 and fac2, was also tested for the SVOC volatility bins under which the IVOC scale factor was set to 2.5.~~ ~~Then the fac3 (0, 0.42, 0.27, 0.345, 0.965) which was the average of fac1 and fac2, was also tested for the five volatility bins.~~ The fac1, fac2, and fac3 were applied to the $OM_{si}(CPM)$ emissions for cases S1.1, S1.2, and S1.3, respectively (see Table 43). For an evaluation of the sensitivity of OA outputs to organic CPM emissions, we conducted simulations with different magnitudes of CPM emissions at the 95% and 50% confidence interval. Thus the S2-S3 cases were designed with the uncertainty ranges of $E_{OA}(CPM)/E_{PM2.5}(FPM)$ at 95% confidence interval (73% and 128% of the amounts in S1), and the S4-

313 S5 cases with the uncertainty ranges at 50% confidence interval (90% and 109% of the amounts in S1).
314 Moreover, the contributions of individual emission categories including PP, IN, IR, and TR were
315 quantified by excluding perturbation of other sources in the S6-9 cases. The simulated contributions of
316 CPM emissions to POA, SOA, OA, and PM_{2.5} concentrations were calculated as the improved simulation
317 concentrations after including CPM emissions relative to the base case, divided by the simulations under
318 these scenarios.~~the improved concentrations after including CPM emissions relative to the base case under~~
319 ~~these scenarios.~~

321 2.4 Observational data

322 For the year 2014, the simulation period was from October 6 to November 14, 2014, with the first 8
323 days being the model spin-up time. Field observation data during the episode from October 14 to
324 November 14, 2014, at the Institute of Atmospheric Physics (IAP) (39°58' N, 116°22' E) in Beijing were
325 from Li et al. (2017a) and Xu et al. (2015). Concentrations of aerosol components were measured in PM₁.
326 In order to make a comparison between simulated and observed results, the PM₁/PM_{2.5} ratio of 0.77 was
327 used to calculate the observed component concentrations in PM_{2.5} based on the observations from Xu et
328 al. (2015). To distinguish between SOA and POA, Aerosol Mass Spectrometer (AMS) measurements and
329 the method of Positive Matrix Factorization (PMF) were used by Xu et al. (2015), identifying three POA
330 factors from coal combustion, biomass burning and cooking, and two SOA factors of semi-volatile and
331 low-volatility oxygenated OA. Observation data of organic carbon (OC) on November 3, 2014, at
332 Qianyanzhou (located in Jian city) and Changsha were provided by CERN Atmospheric Science Branch
333 of the Institute of Atmospheric Physics, Chinese Academy of Sciences (Liu et al., 2018). For the year
334 2018, the simulation period included December 1 to 31, 2018, with the first 5 days for model spin-up.
335 The observation values of OC in the BTH2+26 cities were provided by China Environmental Monitoring
336 Station. These cities include Beijing, Tianjin, Anyang, Baoding, Binzhou, Cangzhou, Changzhi, Dezhou,
337 Hebi, Handan, Hengshui, Heze, Jincheng, Jinan, Jining, Jiaozuo, Kaifeng, Liaocheng, Langfang, Puyang,
338 Shijiazhuang, Tangshan, Taiyuan, Xingtai, Xinxiang, Yangquan, Zibo, and Zhengzhou. The OA/OC ratio
339 of 1.4 (Simon et al., 2011) was used to calculate OA concentrations for the comparison with the simulation
340 results. The observed concentrations of PM_{2.5} were collected from the Chinese National Environmental
341 Monitoring Center (CNEMC). Since the PM_{2.5} observation data from December 22 to 26 were missing,
342 the following analysis of PM_{2.5} did not include these five days. The hourly observation data of
343 meteorological factors, including temperature (T), relative humidity (RH), wind speed (WS), and wind

direction (WD), were provided by the China Meteorological Administration (<http://data.cma.cn/site/index.html>).

3 Results and discussion

3.1 Emissions of condensable particulate matter

Emissions of OA in CPM ($E_{OMA}(CPM)$) were comparable to or even exceeded the emissions of filterable $PM_{2.5}$ ($E_{PM_{2.5}}(FPM)$) for most stationary combustion sources, regardless of the differences among these values (Table 2). Therefore, we constructed a new emission inventory by including CPM. The annual emissions of OA in previous and modified emission inventory over China for the year 2014 and 2017 are presented in Fig. 2. The OMA represents the organic matter in the emission input before the further volatility distributions, while OM ($C^* \leq 100 \mu g m^{-3}$) represents the organic matter allocated in the bin of C^* equal to 100 and below after application of the volatility distributions for the fac1, fac2 and fac3 cases. Based on the simulation case settings, OAM (FPM) from all the sectors was multiplied by fac1 (0.5), while OA (CPM) from stationary combustion and mobile sources was multiplied by fac1 (0.5), fac2 (1.57) or fac3 (1.035). In the previous inventory for 2014 without CPM, the emissions of OMA were 3664.6 Gg, approximately equal to 40% of $PM_{2.5}$ emissions. After the inclusion of CPM released by stationary combustion sources in the new inventory, the emissions of OMA were enhanced by a factor of 2 and even exceeded emissions of $FPM_{2.5}$. The dominant contributors of OMA (FCPM) are combustion sources in power plant and industrial sectors, estimated to be 66% (7006.2 Gg) of the total OMA emissions (10531.1 Gg). The emissions of OM ($C^* \leq 100$) remained unchangeable for the open burning, domestic, and industry process sources since they were mostly FPM, while OM ($C^* \leq 100$) for the power plant, industry combustion, and steel sources were variable based on whether fac1, fac2 or fac3 were applied to the CPM. Similarly, the emissions of OA (FCPM) were 3 times those of OA (FPM) for the year 2017. The emissions of OA from power plant, industry combustion, and steel sources increased by 33 times after considering CPM emissions. These results indicate that the inclusion of organic CPM from stationary combustion sources has a major impact on OA emissions and improves contributions of industrial and power sectors to OA emissions.

Notably, the emission estimates of OA in CPM contained uncertainties, mainly attributed to the representativeness and limitations of chosen emission sources. For power plant, industry combustion, and steel sectors, the average ratios of $E_{OA}E_{OM}(CPM)$ to $E_{PM_{2.5}}(FPM)$ were 4.12, 1.38 and 2.80, respectively (Table 3). The estimation of uncertainties related to variabilities in the ratio of $E_{OM}(CPM)$ to $E_{PM_{2.5}}$

(FPM) was described in section 2.3. Overall, the uncertainty range of $E_{\text{OA}}E_{\text{OM}}(\text{CPM})$ related to variabilities in the ratio of $E_{\text{OA}}(\text{CPM})$ to $E_{\text{PM}_{2.5}}(\text{FPM})$ was -27% ~ +28% at the 95% confidence interval. On this basis, a series of sensitivity cases with different emission ratios were set to determine the uncertainty ranges of CPM contributions (Table 43). In the future, actual measurements of organic CPM emissions from various sources and source-specific identification of volatility distributions are needed to reduce uncertainties in emission estimates.

3.2 Meteorological evaluation

Comparisons between simulated and observed hourly meteorological variables including T, RH, WS, and WD from October 14 to November 14, 2014, at the Beijing site are displayed in Fig. S1. Results show that the model reproduced the hourly variations of T and RH reasonably well, although the maximum and minimum T, and RH did not totally match the observed values. The simulated WS were overestimated, but the hourly changes were reproduced. The variations of WD were not well captured, but the magnitudes of simulated WD were consistent with the observations over the whole period. A more detailed model evaluation for meteorological variables during October 14–November 14, 2014 and December 1–30, 2018 at 9 cities over China is given in Table S1. MB, GE, RMSE denote the bias, root mean square error, and fractional error, respectively, and R refers to the correlation coefficient between observed and simulated results. For the Beijing site in 2014, the MB of T was -0.3 °C, indicating a small deviation of modeled temperature. Good correlations between simulation and observation were shown for T, RH, and WS with R values of 0.90, 0.75, and 0.62, respectively. For all these cities, T, RH, and WS had the R values of 0.83–0.94, 0.67–0.89, and 0.21–0.70 during the study period in 2014, respectively. The R values for T, RH, and WS in 2018 were 0.74–0.95, 0.52–0.85, and 0.33–0.75, respectively. The GE and RMSE of WS were lower than model performance criteria (2 m/s) (Emery et al., 2001) for most cities, displaying relatively good simulations of wind speed. In summary, the WRF model showed a relatively consistent simulation performances of meteorological variables.

3.3 Effects of CPM emissions on POA and SOA concentrations

For the hourly observed and simulated SOA and POA concentrations at the Beijing site, Figs. 3 and 4 show obvious improvements of SOA and POA levels after the consideration of CPM contributions. The specific model species for POA and SOA are shown in Table S4. In all the simulation scenarios, five complete ascending and descending SOA episodes in Fig. 3 were well captured, with much lower mean

406 bias between observations and simulations than previous results of Li et al. (2017a). Three pollution
407 episodes ~~processes~~ before the APEC were clearly captured by the model. The third ~~episode process~~
408 (October 27–November 1) had lower observed SOA levels relative to the first (October 16–21) and second
409 ~~episodes processes~~ (October 22–26), attributed to lower precursor emission concentrations, lower
410 temperature, and regional transports by strong northerly winds on October 26. During the APEC, there
411 were two pollution episodes with lower SOA concentrations due to the effects of emission controls and
412 meteorological conditions (Ansari et al., 2019; Liang et al., 2017). Compared to the observed values,
413 cases without CPM exhibited varying degrees of overestimation or underestimation for SOA and POA.
414 For example, in the ~~AERO7_def base~~ case, the maximum SOA values were overestimated by 50% in the
415 first episodes and up to 65% in the second episodes, while the simulated hourly POA values varied in the
416 range of 0.12~19.06 $\mu\text{g m}^{-3}$, much lower than POA observations during the whole time period. ~~while the~~
417 ~~POA values were largely underestimated by an average of 73% during the whole time period. Then we~~
418 ~~revised the scale factor of IVOC in the AERO7_adj case (see Table 3). The overestimated SOA in the~~
419 ~~AERO7_def for the first and third episodes were reduced by 65% and 60%, respectively.~~ In comparison,
420 the AERO6VBS case underpredicted SOA by up to 65%, and simulated low levels of POA during the
421 first three periods and high levels in the last two episodes. ~~The base case in the following discussions~~
422 ~~referred to AERO7_adj.~~ Overall, the base case underestimated the average POA ~~and~~ SOA and OA levels
423 by 74%, 56% and 65% ~~76% and 66%~~ (Table 45), respectively, emphasizing the potential contributions of
424 missing CPM sources.

425 After considering organic CPM emissions, the underestimation of average POA and SOA was
426 reduced to 37% and 15% under the S1.1 scenario, respectively (Table 5). From the simulated hourly
427 variations in the S1.1 case (Fig. 3), SOA concentrations were enhanced by factors of 0.01~1.86 relative
428 to base case, more consistent with the observations. The gap between average simulations and
429 observations decreased from -9.84 to -2.61 $\mu\text{g m}^{-3}$ (73% decrease). For the peak values in the first, second,
430 fourth, and fifth pollution episodes, the improvements in the peak SOA concentrations were
431 approximately 30, 30, 10, and 15 $\mu\text{g m}^{-3}$. Nevertheless, the overestimation of SOA occurred in the third
432 process, mainly due to meteorological conditions considering the fact that the observed and modeled wind
433 directions were inconsistent during this period as shown in Fig. S1. The prevailing southerly and northeast
434 wind directions in the model during the third process did not bring clean air from the northwest boundary
435 to dilute the local generated SOA (Li et al., 2016, 2019). Also, higher simulated wind speeds transported
436 more precursors with the southerly and northeast winds and caused the overestimation of SOA (see Fig.

437 S1). Correspondingly, the hourly POA simulation concentrations in the S1.1 case increased by 0.07~3.70
438 times compared to the base case, narrowing the average gap between simulations and observations from
439 -11.97 to -6.01 $\mu\text{g m}^{-3}$ (50% decrease), but the high observed levels of POA were still not attained under
440 this scenario. Comparatively, the S1.2 case presented similar hourly simulation results of SOA to the S1.1
441 case with the enhancement by factors of 0.02~2.21 versus the base case, while the simulated POA values
442 were nearly 1.3 times higher than the S1.1 case, capturing most of the high observations throughout the
443 whole study period. Under the S1.3 scenario using different SVOCs parameters from the S1.1 case, the
444 simulation concentrations of SOA were 4% higher and POA were 61% higher than those under the S1.1
445 scenario as shown in Table 5. Based on the evaluation results, the S1.3 scenario showed the optimal
446 improvement effects, with the mean biases of 1.23% for POA and -11.68% for SOA (see Table 5). In
447 consideration of the uncertainty ranges of CPM emissions, a series of sensitivity cases with different
448 emission ratios were conducted. Under the minimum emission scenario in the S2.1 case, the average SOA
449 and POA concentrations were 12%, and 15% lower than those in the S1.1 case, respectively. Under the
450 maximum emission scenario in the S3.1 case, the average SOA and POA concentrations were 14% and
451 19% higher than those in the S1.1 case, respectively. Thus the model can resolve 63% (54%~75%) of the
452 observed POA concentrations and 85% (75%~97%) of the observed SOA concentrations in the cases S1.1
453 (S2.1, S3.1). Then the S2.2 and S3.2 cases applied the same S/IVOCs parameters as S1.2, and also
454 displayed similar results of SOA to those in the S2.1 and S3.1 cases, respectively. Under this setting, the
455 uncertainty ranges were -13% to +13% for SOA, and -22% to +24% for POA in the S1.2 case as shown
456 in Table 5. For the S4.2 and S5.2 cases with the CPM emissions at 50% confidence interval, their SOA
457 concentrations showed small changes with 5% lower in the S4.2 case and 4% higher in the S5.2 case than
458 the S1.2 case; similar minor sensitivity of 8% decrease (S4.2) and 7% increase (S5.2) were found for
459 POA. To explore the contribution of each source category to SOA and POA and identify the key
460 anthropogenic sources of CPM, we conducted simulations with the different separate inputs (S6~S9) (see
461 Table 4). Results show that the CPM emissions from the IR sector made the largest contribution to the
462 POA and SOA increases, accounting for 59% of POA and 55% of SOA, followed by PP (26% for POA
463 and 30% for SOA) and IN sources (13% for POA and 14% for SOA). This was consistent with the
464 differences in the CPM emissions from the above three source sectors (Fig. 2). The sensitivities of SOA
465 and POA to the emission ratio of organic CPM from the TR sector were very small, indicating a weak
466 impact on OA due to small contributions of transportation sources to the OA emissions in FCPM. The
467 above results demonstrate that CPM from stationary sources was an important source for both POA and

468 SOA formations. In summary, when considering the uncertainties of organic CPM emissions, CPM can
469 be a significant contributor to OA concentrations, with the contributions of 58% (51%, 65%) to POA, 49%
470 (42%, 55%) to SOA, 53% (45%, 59%) to OA under the S1.1 (S2.1, S3.1) scenario, and 82% (76%, 85%)
471 to POA, 53% (45%, 58%) to SOA, 70% (63%, 75%) to OA under the S1.2 (S2.2, S3.2) scenario. The
472 S1.3 scenario had the best improvement performance with CPM contributing 74% to POA, 51% to SOA,
473 and 63% to OA.

474 Because of the better representations of temporal variations of SOA and POA after including CPM
475 emissions, OA simulations were correspondingly improved. To separate the effects of CPM on OA into
476 different process contributions, we compared simulation results of these sensitivity cases as shown in Fig.
477 5. The OA composition contains POA, ASOA (SOA from anthropogenic VOCs), BSOA (SOA from
478 biogenic VOCs), and SISOA (SOA from S/IVOCs). The difference between simulations and observations
479 decreased from 21.81 $\mu\text{g m}^{-3}$ in the base case to 8.63 $\mu\text{g m}^{-3}$ in the S1.1 case (60% decrease), with the
480 uncertainty of 11.92 $\mu\text{g m}^{-3}$ (45% decrease in S2.1) to 4.66 $\mu\text{g m}^{-3}$ (79% decrease in S3.1) relative to the
481 base case. However, these cases still underestimated the observed OA levels. The S1.2, S2.2 and S3.2
482 cases increased the contributions of CPM to OA by 14.01, 10.24, 17.92 $\mu\text{g m}^{-3}$ compared to S1.1, S2.1
483 and S3.1, respectively. Notably, the average OA simulations in S1.3 were relatively close to the
484 observations, with the average CPM contributions of 19.98 $\mu\text{g m}^{-3}$ and a minor underestimation of 5.43%
485 (see Table 5). Taking OA composition into account, POA and SISOA accounted for the largest part in all
486 these scenarios. The effects of CPM were only reflected in the enhancements of POA and SISOA. These
487 results suggest that OA was sensitive to the emissions of organic CPM, so it is required to reduce emission
488 uncertainties for better simulations. To sum up, the revised simulations after the inclusion of CPM from
489 stationary combustion and mobile sources led to improved modeling performances of OA during the
490 winter haze episodes, revealing a significant contribution of CPM to atmospheric OA.

491 492 **3.4 Effects of CPM on OA and PM_{2.5} concentrations**

493 To ensure the accuracy and reliability of our modeling results, further studies in other cities were
494 presented. Fig. 6 shows large contributions of CPM to OA on November 3, 2014, at Changsha and
495 Qianyanzhou. After the inclusion of CPM effects in the S1.1, S1.2 and S1.3 cases versus the base case,
496 the simulated OA concentrations were improved by 6.28, 15.80 and 9.60 $\mu\text{g m}^{-3}$ for Changsha,
497 respectively. The simulated OA concentrations increased by 7.06, 15.28 and 10.14 $\mu\text{g m}^{-3}$ in the S1.1,
498 S1.2 and S1.3 cases versus the base case for Qianyanzhou, respectively. Comparatively, the S1.2 case

499 contributed to greater increases of OA concentrations, narrowing the simulation-observation bias from
500 79% to less than 40% for Changsha and more than 70% to less than 25% for Qianyanzhou. The remaining
501 bias was probably attributed to the underestimation of our estimated CPM emissions, effects of
502 meteorological factors and other missing SOA formation pathways.~~the effects of meteorological factors.~~

503 The impacts of CPM on OA were studied during December 6–30, 2018, in the BTH 2+26 cities.
504 Likewise, the improvements in daily OA simulation concentrations can be found at the four studied cities
505 after the consideration of CPM, especially for high pollution days (Fig. 7). The modeled underestimations
506 of OA were improved from -60.88% to -22.55%, -56.47% to -7.91%, -68.38% to -30.51%, and -62.84%
507 to -24.99% with the inclusion of CPM emissions in the S1.1 case relative to the base case for Handan,
508 Shijiazhuang, Xingtai and Dezhou, respectively (Table 5). The contributions of CPM emissions to total
509 OA concentrations reached up to 49%, 53%, 54%, and 50% for Handan, Shijiazhuang, Xingtai, and
510 Dezhou, respectively. Under the S1.3 scenario, the OA simulations showed greater increases, and slightly
511 exceeded observation values with the mean biases of 8.00%, 37.42%, 0.81%, and 2.21% for the above
512 four cities, respectively. For example, daily OA levels in Handan increased by 5.60~57.89 $\mu\text{g m}^{-3}$ after
513 including CPM effects (S1.1 versus base case). On average, the inclusion of CPM doubled the OA
514 concentrations. However, some observations were not captured, while the observed value on December
515 20 was overestimated, indicating uncertainties of the estimated organic CPM emissions. Under the S1.3
516 scenario, the average simulated OA concentrations were enhanced by 1.8 times relative to the base case,
517 with a good capture of some underestimated values in the S1.1 case. For Shijiazhuang with daily OA
518 concentrations below 80 $\mu\text{g m}^{-3}$, the base case underestimated OA levels by 12~78%. After incorporating
519 the CPM emissions in the S1.1 case, the daily OA concentrations were significantly improved by factors
520 of 0.7~1.7. Some observed high values of OA were well captured in the S1.1 case on December 10 with
521 the simulation of 67.75 $\mu\text{g m}^{-3}$ versus observation of 58.65 $\mu\text{g m}^{-3}$, and on December 14 and 30. Under
522 the S1.3 scenario, the daily OA levels increased by factors of 1.3~3.6 relative to the base case. Although
523 the average OA concentrations were somewhat overestimated in the S1.3 case, good agreements between
524 observations and simulations existed on some days, including December 9, 12, 13, 16-19, and 24. For
525 Xingtai, the simulated OA concentrations were enhanced by factors of 1.0~1.8 in the S1.1 case relative
526 to the base case. The model can resolve 69% of average OA observations in the S1.1 case when the
527 emissions of CPM were included. The average OA simulation value was improved by 29.21 $\mu\text{g m}^{-3}$ in the
528 S1.3 case compared to the base case. Then Dezhou showed similar results with the enhancement of
529 0.7~1.6 times for daily OA contributed by CPM in S1.1. Although the observed high OA concentrations

530 exceeding $80 \mu\text{g m}^{-3}$ on December 11 and 16 were not captured in the S1.1 case, the bias between
531 simulation and observation was reduced to -21.92 and $-25.63 \mu\text{g m}^{-3}$ versus -59.17 and $-52.64 \mu\text{g m}^{-3}$ in
532 the base case, respectively. The underestimations of high OA levels on December 11 and 16 were resolved
533 in the S1.3 case, and the average concentration over the whole period was very close to the observation.
534 Table S2 shows the model evaluation results for $\text{PM}_{2.5}$ concentrations under different sensitivity
535 simulation cases. Dezhou was not included due to the missing data. After including the CPM emissions
536 in the S1.1 case, the model can resolve 86%, 86%, and 72% of average $\text{PM}_{2.5}$ observations with increases
537 in $\text{PM}_{2.5}$ concentrations by 32%, 37%, and 38% relative to the base case for Handan, Shijiazhuang, and
538 Xingtai, respectively. $\text{PM}_{2.5}$ simulations were further enhanced for these four cities in the S1.3 case with
539 the NMB values of 2.04%, 7.21%, and -12.08%, respectively. It was notable that the emissions of
540 inorganic components in CPM were not investigated in this study, which can cause modeling deviation.
541 Other factors including boundary layer height and wind can also affect the simulations. In summary, our
542 estimated CPM emissions showed a reasonable range, which can make a significant contribution to
543 atmospheric OA and $\text{PM}_{2.5}$.

544

545 **3.5 Regional contributions of CPM to OA and $\text{PM}_{2.5}$**

546 The regional effects of CPM emissions on atmospheric OA and $\text{PM}_{2.5}$ from a nationwide perspective
547 were investigated. The concentrations of POA, SOA and OA averaged over the whole study period from
548 October 14 to November 14, 2014, showed varying degrees of regional increases after incorporating CPM
549 emissions, mainly in central and eastern regions in China (Fig. 8). In the base case, the simulation values
550 of POA and SOA were both lower than $14 \mu\text{g m}^{-3}$ over China. Correspondingly, OA concentrations did
551 not exceed $22 \mu\text{g m}^{-3}$ with the maximum values distributed in the BTH region and Central China. After
552 the consideration of CPM effects in the S1.1 case relative to the base case, the concentrations of POA,
553 SOA and OA substantially increased over North China, East China, and Central China including Beijing,
554 Tianjin, Shanghai, and provinces of Liaoning, Shandong, Shanxi, Henan, Hubei, Anhui, Jiangsu, Zhejiang,
555 Hunan, Jiangxi. The most remarkable enhancement values were up to 10, 12, and $20 \mu\text{g m}^{-3}$ for POA,
556 SOA and OA, respectively. Then under the S1.2 scenario with the same emissions as the S1.1 case but
557 different SIVOCs parameterization, substantial increases in the POA simulations by more than $16 \mu\text{g m}^{-3}$
558 were found for most cities in North China, East China, and Central China, with the maximum distributed
559 in the BTH region (up to $24 \mu\text{g m}^{-3}$), attributable to large amounts of emissions from industrial plants and
560 power plants in this region. The OA concentrations for many cities located in North China and East China

561 increased by more than $24 \mu\text{g m}^{-3}$ after including CPM emissions in the S1.2 case. Since the contributions
562 of CPM to SOA in the S1.2 case were only slightly larger than those in the S1.1 case, the greater
563 improvements of OA in S1.2 mainly result from the POA increases. The regional increases in the POA,
564 SOA and OA simulations in the S1.3 case were not lower than 10, 8, and $18 \mu\text{g m}^{-3}$ for most cities in
565 North China, East China, and Central China, respectively.

566 The regional contributions of organic CPM emissions to $\text{PM}_{2.5}$ concentrations were explored in the
567 BTH2+26 cities averaged over the period from December 6 to 30, 2018 (Fig. 9). In the base case without
568 the CPM effects, the model comparisons against observations suggest that $\text{PM}_{2.5}$ levels were greatly
569 underestimated in almost all cities except Tangshan (Fig. 9a). Several cities with observed $\text{PM}_{2.5}$
570 concentrations higher than $80 \mu\text{g m}^{-3}$ showed the greatest underestimations with simulation values under
571 $50 \mu\text{g m}^{-3}$. Under the S1.1 scenario including CPM emissions, the simulated $\text{PM}_{2.5}$ concentrations were
572 substantially enhanced in almost all the studied cities, closer to the observations (Fig. 9b). The
573 contributions of CPM to $\text{PM}_{2.5}$ were not lower than $14 \mu\text{g m}^{-3}$ for the most cities (Fig. 9c). Under the S1.3
574 scenario, CPM made a significant contribution to $\text{PM}_{2.5}$ concentrations, more than $24 \mu\text{g m}^{-3}$ for most
575 cities (Fig. 9f). High observations for Baoding, Shijiazhuang, Xingtai, Hengshui, Dezhou and Handan
576 were well captured (Fig. 9e). The scatter plots of observed and simulated daily $\text{PM}_{2.5}$ concentrations for
577 all BTH2+26 cities in Fig. 9d show obvious improvement in $\text{PM}_{2.5}$ simulations after including CPM
578 emissions, with the NMB values from -32.4% in the base case to -10.6% in the S1.1 case, and then to 5.5%
579 in the S1.3 case. Nevertheless, there were still model-measurement biases for $\text{PM}_{2.5}$ concentrations in
580 some cities with high observations exceeding $90 \mu\text{g m}^{-3}$, including Baoding, Anyang, Puyang, Heze,
581 Zhengzhou and Kaifeng. The insufficient improvement of $\text{PM}_{2.5}$ can be attributed to incomplete emission
582 information of inorganic components, which need further research. In addition, some heavy pollution
583 hours were chosen to investigate the regional impacts of CPM on $\text{PM}_{2.5}$ concentrations, including 8:00,
584 9:00, 10:00, 11:00, and 21:00 on December 15 (Fig. 10a). Besides the BTH2+26 cities, some surrounding
585 cities (Chaoyang, Chengde, Datong, Dongying, Huludao, Jinzhou, Linxi, Luoyang, Luohe, Qinhuangdao,
586 Qindao, Rizhao, Sanmenxia, Shangqiu, Shuozhou, Taian, Weihai, Weifang, Xinzhou, Xinyang, Yantai,
587 Zaozhuang, Zhangjiakou, Zhoukou, Zhunmadian) were also included. Results show that the
588 underestimated $\text{PM}_{2.5}$ concentrations in the base case were substantially improved after considering CPM
589 emissions in S1.1 and S1.3, especially for some high observations over $170 \mu\text{g m}^{-3}$. Better agreement
590 between simulated and observed $\text{PM}_{2.5}$ concentrations for all these cities was achieved, with the NMB
591 values from -32.6% in the base case to -12.3% in S1.1, and to 0.6% in S1.3 (Fig. 10b). To sum up, the

592 consideration of CPM effects can improve the underestimation of regional OA and PM_{2.5} simulations to
593 a certain extent, especially during the heavy pollution periods.

594 595 **4 Conclusions**

596 In this study, we focused on emissions of condensable PM from stationary combustion and mobile
597 sources and developed an emission inventory of organic CPM in China. Using emission inputs with and
598 without CPM contributions, the CMAQ model was applied to simulate the impacts of CPM on
599 atmospheric OA and PM_{2.5} in China. The results show that the inclusion of CPM emissions increased
600 annual OA emissions by a factor of 2 for both the years 2014 and 2017. The power plant, industry
601 combustion, and steel sectors in the stationary combustion sources dominated OA emissions in the new
602 inventory. A series of sensitivity scenarios with different emission ratios and volatility distributions show
603 that CPM contributed significantly to the improvement of hourly SOA and POA concentrations during
604 the period from October 14 to November 14, 2014, at Beijing. The contributions of CPM were 51 ~ 85%
605 to POA and 42 ~ 58% to SOA under these scenarios. The model comparison against observations suggests
606 that the consideration of CPM effects improved the underestimations of simulation results and achieved
607 a good capture of peak SOA and POA values. In addition, the enhancements of daily OA levels by CPM
608 were demonstrated during December 6-30, 2018 at Handan, Shijiazhuang, Xingtai and Dezhou.
609 Compared to daily observations, the NMB values in these four cities were improved from -60.88%, -
610 56.47%, -68.38%, -62.84% (the base case) to -22.55%, -7.91%, -30.51%, -24.99% (the S1.1 case) for
611 POA, SOA and OA, respectively. The regional contributions of CPM also narrowed the gap between
612 simulated and observed concentrations of PM_{2.5} in the BTH2+26 cities. In conclusion, our estimated CPM
613 emissions contributed significantly to the improvements of simulation performances for both atmospheric
614 OA and PM_{2.5}, especially during the high pollution episodes. Therefore, the CPM emissions can be
615 incorporated into chemical transport models together with FPM to improve the simulation accuracies of
616 OA and PM_{2.5}.

617 Our estimates of organic CPM emissions and SOA formation from CPM contained the following
618 uncertainties: (1) The construction of the organic CPM emission inventory in the present study was based
619 on the ratios of $E_{\text{POA}}(\text{CPM})$ to $E_{\text{PM}_{2.5}}(\text{FPM})$ derived from limited sources, instead of the actual
620 measurement data of CPM emissions from the different sources and regions over China. (2) Since there
621 was no explicit volatility characterization of primary organic CPM species available for incorporation
622 into the emission inventories, the S/IVOCs emissions were scaled to the POA emissions. (3) Due to the

623 lack of relevant data, the original surrogate species of S/IVOCs and their properties in the CMAQ model
624 remained unchanged for representing the SOA formation from CPM, rather than introducing new model
625 species with identified parameters related to OH reaction rates, effective saturation concentration, and
626 multigenerational aging products. Based on these limitations, it is strongly recommended that future
627 studies conduct extensive surveys of CPM emissions from various stationary combustion sources and
628 measure the actual emissions of source-specific and region-specific S/IVOCs to better constrain OA
629 simulations by chemical transport models.

630
631 **Data availability.** The emission data and model results are available upon request.

632 **Supplement.** The supplement related to this article is available online.

633 **Author contributions.** S.Y., P.L. conceived and designed the research. M. L. performed model simulations.
634 M. L., X. C., Y. Z., and Z. L. conducted data analysis. Z. S., W. L., X. Z, B. N. M., K. A., R. M., D. R.,
635 and J. H. S contributed to the scientific discussions. M. Z, Y. S., Z. L., and C. S. provided observation
636 data. S. W. provided the Abacas emission data. S. Y., M. L, P. L., and J. H. S wrote and revised the
637 manuscript.

638 **Competing interests.** The authors declare that they have no conflict of interest.

639 **Disclaimer.** The views expressed in this article are those of the authors and do not necessarily represent
640 the views or policies of the U.S. Environmental Protection Agency.

641 **Acknowledgements.** The authors would like to thank Comprehensive data collection and sharing platform
642 for atmospheric environmental science (<https://napcdata.craes.cn>), and CERN Atmospheric Science
643 Branch of the Institute of Atmospheric Physics, Chinese Academy of Sciences for providing OC
644 measurement data.

645 **Financial support.** This study is supported by the National Natural Science Foundation of China (No.
646 42175084, 21577126, 41561144004, and 92044302), Department of Science and Technology of China
647 (No. 2018YFC0213506 and 2018YFC0213503), and National Research Program for Key Issues in Air
648 Pollution Control in China (No. DQGG0107). Pengfei Li is supported by National Natural Science
649 Foundation of China (No. 22006030), Initiation Fund for Introducing Talents of Hebei Agricultural
650 University (412201904), and Hebei Youth Top Fund (BJ2020032).

651 **References**

- 652 Ansari, T. U., Wild, O., Li, J., Yang, T., Xu, W., Sun, Y. and Wang, Z.: Effectiveness of short-term air quality emission
653 controls: a high-resolution model study of Beijing during the Asia-Pacific Economic Cooperation (APEC) summit
654 period, *Atmos. Chem. Phys.*, 19(13), 8651–8668, doi:10.5194/acp-19-8651-2019, 2019.

655 Appel, K. W., Bash, J. O., Fahey, K. M., Foley, K. M., Gilliam, R. C., Hogrefe, C., Hutzell, W. T., Kang, D., Mathur, R.,
656 Murphy, B. N., Napelenok, S. L., Nolte, C. G., Pleim, J. E., Pouliot, G. A., Pye, H. O. T., Ran, L., Roselle, S. J.,
657 Sarwar, G., Schwede, D. B., Sidi, F. I., Spero, T. L. and Wong, D. C.: The Community Multiscale Air Quality (CMAQ)
658 model versions 5.3 and 5.3.1: System updates and evaluation, *Geosci. Model Dev.*, 14(5), 2867–2897,
659 doi:10.5194/gmd-14-2867-2021, 2021.

660 Carlton, A. G. and Baker, K. R.: Photochemical modeling of the ozark isoprene volcano: MEGAN, BEIS, and their
661 impacts on air quality predictions, *Environ. Sci. Technol.*, 45(10), 4438–4445, doi:10.1021/es200050x, 2011.

662 Carlton, A. G., Wiedinmyer, C. and Kroll, J. H.: A review of Secondary organic aerosol (SOA) formation from isoprene,
663 *Atmos. Chem. Phys.*, 9(14), 4987–5005, doi:10.5194/acp-9-4987-2009, 2009.

664 Chen, L., Zhu, J., Liao, H., Gao, Y., Qiu, Y., Zhang, M., Liu, Z., Li, N. and Wang, Y.: Assessing the formation and
665 evolution mechanisms of severe haze pollution in the Beijing-Tianjin-Hebei region using process analysis, *Atmos.*
666 *Chem. Phys.*, 19(16), 10845–10864, doi:10.5194/acp-19-10845-2019, 2019.

667 Choi, Y. J. and Fernando, H. J. S.: Implementation of a windblown dust parameterization into MODELS-3/CMAQ:
668 Application to episodic PM events in the US/Mexico border, *Atmos. Environ.*, 42(24), 6039–6046,
669 doi:10.1016/j.atmosenv.2008.03.038, 2008.

670 Corio, L.A., Sherwell, J.: In-stack condensible particulate matter measurements and issues. *J. Air Waste Manage. Assoc.*
671 50, 207–218, 2000.

672 Donahue, N. M., Robinson, A. L., Stanier, C. O., and Pandis, S. N.: Coupled partitioning, dilution, and chemical aging of
673 semivolatile organics, *Environ. Sci. Technol.*, 40, 2635–2643, <https://doi.org/10.1021/es052297c>, 2006.

674 Donahue, N. M., Epstein, S. A., Pandis, S. N., and Robinson, A. L.: A two-dimensional volatility basis set: 1. organic-
675 aerosol mixing thermodynamics, *Atmos. Chem. Phys.*, 11, 3303–3318, <https://doi.org/10.5194/acp-11-3303-2011>, 2011.

676 Dong, Z., Wang, S., Xing, J., Chang, X., Ding, D. and Zheng, H.: Regional transport in Beijing-Tianjin-Hebei region and
677 its changes during 2014–2017: The impacts of meteorology and emission reduction, *Sci. Total Environ.*, 737, 139792,
678 doi:10.1016/j.scitotenv.2020.139792, 2020.

679 Emery, C., Tai, E. and Yarwood, G.: Enhanced meteorological modeling and performance evaluation for two Texas ozone
680 episodes, Texas Natural Resource Conservation Commission, ENVIRON International Corporation, pp. 1–235.
681 Available online: [http://www.tceq.state.tx.us/assets/public/implementation/air/am/contracts/reports/mm/
682 EnhancedMetModelingAndPerformanceEvaluation.pdf](http://www.tceq.state.tx.us/assets/public/implementation/air/am/contracts/reports/mm/EnhancedMetModelingAndPerformanceEvaluation.pdf).

683 EPA, United States Environmental Protection Agency, Method 202 A – Dry Impinger Method for Determining
684 Condensable Particulate Emissions from Stationary Sources, 2017.

685 Feng, Y., Li, Y., Cui, L.: Critical review of condensable particulate matter, *Fuel*, 224, 801–813, 2018.

686 Feng, Y., Li, Y., Zhang, X., Su, S., Zhang, Z., Gan, Z. and Dong, Y.: Comparative study on the characteristics of
687 condensable particulate matter emitted from three kinds of coal, *Environ. Pollut.*, 270, 116267,
688 doi:10.1016/j.envpol.2020.116267, 2021.

689 Fu, T. M., Cao, J. J., Zhang, X. Y., Lee, S. C., Zhang, Q., Han, Y. M., Qu, W. J., Han, Z., Zhang, R., Wang, Y. X., Chen,
690 D. and Henze, D. K.: Carbonaceous aerosols in China: Top-down constraints on primary sources and estimation of
691 secondary contribution, *Atmos. Chem. Phys.*, 12(5), 2725–2746, doi:10.5194/acp-12-2725-2012, 2012.

692 Fuzzi, S., Andreae, M. O., Huebert, B. J., Kulmala, M., Bond, T. C., Boy, M., Doherty, S. J., Guenther, A., Kanakidou,
693 M., Kawamura, K., Kerminen, V. M., Lohmann, U., Russell, L. M. and Pöschl, U.: Critical assessment of the current
694 state of scientific knowledge, terminology, and research needs concerning the role of organic aerosols in the
695 atmosphere, climate, and global change, *Atmos. Chem. Phys.*, 6(7), 2017–2038, doi:10.5194/acp-6-2017-2006, 2006.

696 Gao, M., Carmichael, G. R., Wang, Y., Saide, P. E., Yu, M., Xin, J., Liu, Z. and Wang, Z.: Modeling study of the 2010
697 regional haze event in the North China Plain, *Atmos. Chem. Phys.*, 16(3), 1673–1691, doi:10.5194/acp-16-1673-2016,
698 2016.

699 Gehring, U., Gruzjeva, O., Agius, R. M., Beelen, R., Custovic, A., Cyrys, J., Eeftens, M., Flexeder, C., Fuertes, E.,
700 Heinrich, J., Hoffmann, B., de Jongste, J. C., Kerkhof, M., Klümper, C., Korek, M., Mäder, A., Schultz, E. S., Simpson,
701 A., Sugiri, D., Svartengren, M., von Berg, A., Wijga, A. H., Pershagen, G. and Brunekreef, B.: Air pollution exposure

702 and lung function in children: The ESCAPE project, *Environ. Health Perspect.*, 121(11–12), 1357–1364,
703 doi:10.1289/ehp.1306770, 2013.

704 Van Der Gon, H. A. C. D., Bergström, R., Fountoukis, C., Johansson, C., Pandis, S. N., Simpson, D. and Visschedijk, A. J.
705 H.: Particulate emissions from residential wood combustion in Europe - revised estimates and an evaluation, *Atmos.*
706 *Chem. Phys.*, 15(11), 6503–6519, doi:10.5194/acp-15-6503-2015, 2015.

707 Grieshop, A. P., Logue, J. M., Donahue, N. M. and Robinson, A. L.: Laboratory investigation of photochemical oxidation
708 of organic aerosol from wood fires 1: measurement and simulation of organic aerosol evolution, *Atmos. Chem. Phys.*,
709 9, 1263–1277, 2009.

710 Han, Z., Xie, Z., Wang, G., Zhang, R. and Tao, J.: Modeling organic aerosols over east China using a volatility basis-set
711 approach with aging mechanism in a regional air quality model, *Atmos. Environ.*, 124, 186–198,
712 doi:10.1016/j.atmosenv.2015.05.045, 2016.

713 Hayes, P. L., Carlton, A. G., Baker, K. R., Ahmadov, R., Washenfelder, R. A., Alvarez, S., Rappenglück, B., Gilman, J.
714 B., Kuster, W. C., De Gouw, J. A., Zotter, P., Prévôt, A. S. H., Szidat, S., Kleindienst, T. E., Offenberg, J. H., Ma, P. K.
715 and Jimenez, J. L.: Modeling the formation and aging of secondary organic aerosols in Los Angeles during CalNex
716 2010, *Atmos. Chem. Phys.*, 15(10), 5773–5801, doi:10.5194/acp-15-5773-2015, 2015.

717 He, X., Wang, Q., Huang, X. H. H., Huang, D. D., Zhou, M., Qiao, L., Zhu, S., Ma, Y. ge, Wang, H. li, Li, L., Huang, C.,
718 Xu, W., Worsnop, D. R., Goldstein, A. H. and Yu, J. Z.: Hourly measurements of organic molecular markers in urban
719 Shanghai, China: Observation of enhanced formation of secondary organic aerosol during particulate matter episodic
720 periods, *Atmos. Environ.*, 240, doi:10.1016/j.atmosenv.2020.117807, 2020.

721 Hu, Y., Feng, Y., Wang, C., Ma, Z. and Jiang, T.: Studies on Monitoring Method of Condensable Particulate and Water-
722 soluble Ions in Fumes from Coal Fired Boilers, *Environ. Monit. Manag. Technol.*, 28(1), 41–45, 2016.

723 Huang, R. J., Zhang, Y., Bozzetti, C., Ho, K. F., Cao, J. J., Han, Y., Daellenbach, K. R., Slowik, J. G., Platt, S. M.,
724 Canonaco, F., Zotter, P., Wolf, R., Pieber, S. M., Bruns, E. A., Crippa, M., Ciarelli, G., Piazzalunga, A., Schwikowski,
725 M., Abbaszade, G., Schnelle-Kreis, J., Zimmermann, R., An, Z., Szidat, S., Baltensperger, U., El Haddad, I. and Prévôt,
726 A. S. H.: High secondary aerosol contribution to particulate pollution during haze events in China, *Nature*, 514(7521),
727 218–222, doi:10.1038/nature13774, 2015.

728 Huang, X., Ding, A., Gao, J., Zheng, B., Zhou, D., Qi, X., Tang, R., Wang, J., Ren, C., Nie, W., Chi, X., Xu, Z., Chen, L.,
729 Li, Y., Che, F., Pang, N., Wang, H., Tong, D., Qin, W., Cheng, W., Liu, W., Fu, Q., Liu, B., Chai, F., Davis, S. J.,
730 Zhang, Q. and He, K.: Enhanced secondary pollution offset reduction of primary emissions during COVID-19
731 lockdown in China, *Natl. Sci. Rev.*, 8(2), doi:10.1093/nsr/nwaa137, 2021.

732 Jathar, S. H., Woody, M., Pye, H. O. T., Baker, K. R. and Robinson, A. L.: Chemical transport model simulations of
733 organic aerosol in southern California: Model evaluation and gasoline and diesel source contributions, *Atmos. Chem.*
734 *Phys.*, 17(6), 4305–4318, doi:10.5194/acp-17-4305-2017, 2017.

735 Kanakidou, M., Seinfeld, J. H., Pandis, S. N., Barnes, I., Dentener, F. J., Facchini, M. C., Van Dingenen, R., Ervens, B.,
736 Nenes, A., Nielsen, C. J., Swietlicki, E., Putaud, J. P., Balkanski, Y., Fuzzi, S., Horth, J., Moortgat, G. K., Winterhalter,
737 R., Myhre, C. E. L., Tsigaridis, K., Vignati, E., Stephanou, E. G. and Wilson, J.: Organic aerosol and global climate
738 modelling: A review, *Atmos. Chem. Phys.*, 5(4), 1053–1123, doi:10.5194/acp-5-1053-2005, 2005.

739 Kroll, J. H. and Seinfeld, J. H.: Chemistry of secondary organic aerosol: Formation and evolution of low-volatility
740 organics in the atmosphere, *Atmos. Environ.*, 42(16), 3593–3624, doi:10.1016/j.atmosenv.2008.01.003, 2008.

741 Lane, T. E., Donahue, N. M. and Pandis, S. N.: Simulating secondary organic aerosol formation using the volatility basis-
742 set approach in a chemical transport model, *Atmos. Environ.*, 42(32), 7439–7451, doi:10.1016/j.atmosenv.2008.06.026,
743 2008.

744 Li, P. F., Yan, R. C., Yu, S. C., Wang, S., Liu, W. P., and Bao, H. M.: Reinstate regional transport of PM_{2.5} as a major
745 cause of severe haze in Beijing, *Proc Natl Acad Sci USA (PNAS)*, 112(21), E2739–E2740.
746 doi:10.1073/pnas.1502596112., 2015.

747 Li, H., Zhang, Q., Zhang, Q., Chen, C., Wang, L., Wei, Z., Zhou, S., Parworth, C., Zheng, B., Canonaco, F., Prévôt, A. S.
748 H., Chen, P., Zhang, H., Wallington, T. J. and He, K.: Wintertime aerosol chemistry and haze evolution in an extremely

749 polluted city of the North China Plain: Significant contribution from coal and biomass combustion, *Atmos. Chem.*
750 *Phys.*, 17(7), 4751–4768, doi:10.5194/acp-17-4751-2017, 2017a.

751 Li, J., Zhang, M., Wu, F., Sun, Y. and Tang, G.: Assessment of the impacts of aromatic VOC emissions and yields of SOA
752 on SOA concentrations with the air quality model RAMS-CMAQ, *Atmos. Environ.*, 158, 105–115,
753 doi:10.1016/j.atmosenv.2017.03.035, 2017b.

754 Li, J., Qi, Z., Li, M., Wu, D., Zhou, C., Lu, S., Yan, J. and Li, X.: Physical and Chemical Characteristics of Condensable
755 Particulate Matter from an Ultralow-Emission Coal-Fired Power Plant, *Energy and Fuels*, 31(2), 1778–1785,
756 doi:10.1021/acs.energyfuels.6b02919, 2017c.

757 Li, J., Li, X., Zhou, C., Li, M., Lu, S., Yan, J. and Qi, Z.: Study on the Influencing Factors of the Distribution
758 Characteristics of Polycyclic Aromatic Hydrocarbons in Condensable Particulate Matter, *Energy and Fuels*, 31(12),
759 13233–13238, doi:10.1021/acs.energyfuels.7b01991, 2017d.

760 Li, J.: Experimental study on emission characteristics of condensable particulate matter and typical organic pollutants in
761 coal-fired flue gas., Ph.D. thesis, School of Energy Engineering, Zhejiang University, China, 164 pp., 2018.

762 Li, X., Qiao, Y., Zhu, J., Shi, L. and Wang, Y.: The “APEC blue” endeavor: Causal effects of air pollution regulation on
763 air quality in China, *J. Clean. Prod.*, 168, 1381–1388, doi:10.1016/j.jclepro.2017.08.164, 2017e.

764 Li, Y., Ye, C., Liu, J., Zhu, Y., Wang, J., Tan, Z., Lin, W., Zeng, L. and Zhu, T.: Observation of regional air pollutant
765 transport between the megacity Beijing and the North China Plain, *Atmos. Chem. Phys.*, 16(22), 14265–14283,
766 doi:10.5194/acp-16-14265-2016, 2016.

767 Li, X., Zhou, C., Li, J., Lu, S. and Yan, J.: Distribution and emission characteristics of filterable and condensable
768 particulate matter before and after a low-low temperature electrostatic precipitator, *Environ. Sci. Pollut. Res.*, 26(13),
769 12798–12806, doi:10.1007/s11356-019-04570-y, 2019.

770 Li, Y., Tan, Z., Ye, C., Wang, J., Wang, Y., Zhu, Y., Liang, P., Chen, X., Fang, Y., Han, Y., Wang, Q., He, D., Wang, Y.
771 and Zhu, T.: Using wavelet transform to analyse on-road mobile measurements of air pollutants: A case study to
772 evaluate vehicle emission control policies during the 2014 APEC summit, *Atmos. Chem. Phys.*, 19(22), 13841–13857,
773 doi:10.5194/acp-19-13841-2019, 2019.

774 Liang, P., Zhu, T., Fang, Y., Li, Y., Han, Y., Wu, Y., Hu, M. and Wang, J.: The role of meteorological conditions and
775 pollution control strategies in reducing air pollution in Beijing during APEC 2014 and Victory Parade 2015, *Atmos.*
776 *Chem. Phys.*, 17(22), 13921–13940, doi:10.5194/acp-17-13921-2017, 2017.

777 Lin, C. Q., Liu, G., Lau, A. K. H., Li, Y., Li, C. C., Fung, J. C. H. and Lao, X. Q.: High-resolution satellite remote sensing
778 of provincial PM_{2.5} trends in China from 2001 to 2015, *Atmos. Environ.*, 180, 110–116,
779 doi:10.1016/j.atmosenv.2018.02.045, 2018.

780 Liu, Z., Gao, W., Yu, Y., Hu, B., Xin, J., Sun, Y., Wang, L., Wang, G., Bi, X., Zhang, G., Xu, H., Cong, Z., He, J., Xu, J.,
781 and Wang, Y.: Characteristics of PM_{2.5} mass concentrations and chemical species in urban and background areas of
782 china: Emerging results from the CARE-china network, *Atmos. Chem. Phys.*, 18(12), 8849–8871, doi:10.5194/acp-18-
783 8849-2018, 2018.

784 Lu, Q., Zhao, Y., and Robinson, A. L.: Comprehensive organic emission profiles for gasoline, diesel, and gas-turbine
785 engines including intermediate and semi-volatile organic compound emissions, *Atmos. Chem. Phys.*, 18(23), 17637-
786 17654, doi:http://dx.doi.org/10.5194/acp-18-17637-2018, 2018.

787 Lu, C. M., Dat, N. D., Lien, C. K., Chi, K. H. and Chang, M. B.: Characteristics of Fine Particulate Matter and Polycyclic
788 Aromatic Hydrocarbons Emitted from Coal Combustion Processes, *Energy and Fuels*, 33(10), 10247–10254,
789 doi:10.1021/acs.energyfuels.9b02201, 2019.

790 Lu, Q., N. Murphy, B., Qin, M., J. Adams, P., Zhao, Y., O. T. Pye, H., Efstathiou, C., Allen, C. and L. Robinson, A.:
791 Simulation of organic aerosol formation during the CalNex study: Updated mobile emissions and secondary organic
792 aerosol parameterization for intermediate-volatility organic compounds, *Atmos. Chem. Phys.*, 20(7), 4313–4332,
793 doi:10.5194/acp-20-4313-2020, 2020.

794 Morino, Y., Chatani, S., Tanabe, K., Fujitani, Y., Morikawa, T., Takahashi, K., Sato, K. and Sugata, S.: Contributions of
795 Condensable Particulate Matter to Atmospheric Organic Aerosol over Japan, *Environ. Sci. Technol.*, 52(15), 8456–

796 8466, doi:10.1021/acs.est.8b01285, 2018.

- 797 Murphy, B. N. and Pandis, S. N.: Simulating the formation of semivolatile primary and secondary organic aerosol in a
798 regional chemical transport model, *Environ. Sci. Technol.*, 43(13), 4722–4728, doi:10.1021/es803168a, 2009.
- 799 Murphy, B. N., Woody, M. C., Jimenez, J. L., Carlton, A. M. G., Hayes, P. L., Liu, S., Ng, N. L., Russell, L. M., Setyan,
800 A., Xu, L., Young, J., Zaveri, R. A., Zhang, Q. and Pye, H. O. T.: Semivolatile POA and parameterized total
801 combustion SOA in CMAQv5.2: Impacts on source strength and partitioning, *Atmos. Chem. Phys.*, 17(18), 11107–
802 11133, doi:10.5194/ACP-17-11107-2017, 2017.
- 803 Murphy, B. N., Nolte, C. G., Sidi, F., Bash, J. O., Appel, K. W., Jang, C., Kang, D., Kelly, J., Mathur, R., Napelenok, S.,
804 Pouliot, G. and Pye, H. O. T.: The detailed emissions scaling, isolation, and diagnostic (DESID) module in the
805 Community Multiscale Air Quality (CMAQ) modeling system version 5.3.2, *Geosci. Model Dev.*, 14(6), 3407–3420,
806 doi:10.5194/gmd-14-3407-2021, 2021.
- 807 Odum, J. R., Hoffmann, T., Bowman, F., Collins, D., Flagan, R. C. and Seinfeld, J. H.: Gas/Particle Partitioning and
808 Secondary Organic Aerosol Yields, *Environ. Sci. Technol.*, 30, 2580–2585, doi:10.1021/ES950943+, 1996.
- 809 Pankow, J. F.: An absorption model of gas/particle partitioning of organic compounds in the atmosphere, *Atmos. Environ.*,
810 28(2), 185–188, doi:10.1016/1352-2310(94)90093-0, 1994.
- 811 Pei, B.: Determination and emission of condensable particulate matter from coal-fired power plants, *Huanjing*
812 *Kexue/Environmental Sci.*, 36(5), 1544–1549, doi:10.13227/j.hjcx.2015.05.005, 2015.
- 813 Pennington, E., Seltzer, K., Murphy, B., Qin, M., Seinfeld, J. and Pye, H.: Modeling secondary organic aerosol formation
814 from volatile chemical products, *Atmos. Chem. Phys.*, (July), 1–26, doi:10.5194/acp-2021-547, 2021.
- 815 Pope, C. A., Burnett, R. T., Thun, M. J., Calle, E. E., Krewski, D., Ito, K. and Thurston, G. D.: Lung cancer,
816 cardiopulmonary mortality, and long-term exposure to fine particulate air pollution, *J. Am. Med. Assoc.*, 287(9), 1132–
817 1141, doi:10.1001/jama.287.9.1132, 2002.
- 818 Pye, H. O. T., Pinder, R. W., Piletic, I. R., Xie, Y., Capps, S. L., Lin, Y., Surratt, J. D., Zhang, Z., Gold, A., Luecken, D. J.,
819 Hutzell, W. T., Jaoui, M., Offenberg, J. H., Kleindienst, T. E., Lewandowski, M., and Edney, E. O.: Epoxide pathways
820 improve model predictions of isoprene markers and reveal key role of acidity in aerosol formation. *Environmental*
821 *Science & Technology*, 47(19), 11056–11064, <https://doi.org/10.1021/es402106h>, 2013.
- 822 Pye, H. O. T., Murphy, B. N., Xu, L., Ng, N. L., Carlton, A. G., Guo, H., Weber, R., Vasilakos, P., Appel, K. W.,
823 Budisulistiorini, S. H., Surratt, J. D., Nenes, A., Hu, W., Jimenez, J. L., Isaacman-VanWertz, G., Misztal, P. K., and
824 Goldstein, A. H.: On the implications of aerosol liquid water and phase separation for organic aerosol mass, *Atmos.*
825 *Chem. Phys.*, 17, 343–369, <https://doi.org/10.5194/acp-17-343-2017>, 2017.
- 826 Qi, Z., Li, J., Wu, D., Xie, W., Li, X. and Liu, C.: Particulate Matter Emission Characteristics and Removal Efficiencies of
827 a Low-Low Temperature Electrostatic Precipitator, *Energy and Fuels*, 31(2), 1741–1746,
828 doi:10.1021/acs.energyfuels.6b02692, 2017.
- 829 Qin, M., Murphy, B. N., Isaacs, K. K., McDonald, B. C., Lu, Q., McKeen, S. A., Koval, L., Robinson, A. L., Efstathiou,
830 C., Allen, C. and Pye, H. O. T.: Criteria pollutant impacts of volatile chemical products informed by near-field
831 modelling, *Nat. Sustain.*, 4(2), 129–137, doi:10.1038/s41893-020-00614-1, 2021.
- 832 Robinson, A. L., Donahue, N. M., Shrivastava, M. K., Weitkamp, E. A., Sage, A. M., Grieshop, A. P., Lane, T. E., Pierce,
833 J. R. and Pandis, S. N.: Rethinking organic aerosols: Semivolatile emissions and photochemical aging, *Science (80-.)*,
834 315(5816), 1259–1262, doi:10.1126/science.1133061, 2007.
- 835 Shrivastava, M., Fast, J., Easter, R., Gustafson, W. I., Zaveri, R. A., Jimenez, J. L., Saide, P. and Hodzic, A.: Modeling
836 organic aerosols in a megacity: Comparison of simple and complex representations of the volatility basis set approach,
837 *Atmos. Chem. Phys.*, 11(13), 6639–6662, doi:10.5194/acp-11-6639-2011, 2011.
- 838 Shrivastava, M. K., Lane, T. E., Donahue, N. M., Pandis, S. N. and Robinson, A. L.: Effects of gas particle partitioning
839 and aging of primary emissions on urban and regional organic aerosol concentrations, *J. Geophys. Res. Atmos.*,
840 113(18), doi:10.1029/2007JD009735, 2008.
- 841 Simon, H., Bhave, P. V., Swall, J. L., Frank, N. H., and Malm, W. C.: Determining the spatial and seasonal variability in
842 OM/OC ratios across the US using multiple regression. *Atmos. Chem. Phys.*, 11(6), 2933–2949,

843 <https://doi.org/10.5194/acp-11-2933-2011>, 2011.

- 844 Song, J., Lu, S., Wu, Y., Zhou, C., Li, X. and Li, J.: Migration and distribution characteristics of organic and inorganic
845 fractions in condensable particulate matter emitted from an ultralow emission coal-fired power plant, *Chemosphere*,
846 243, 125346, doi:10.1016/j.chemosphere.2019.125346, 2020.
- 847 Sun, Y., Du, W., Wang, Q., Zhang, Q., Chen, C., Chen, Y., Chen, Z., Fu, P., Wang, Z., Gao, Z. and Worsnop, D. R.: Real-
848 Time Characterization of Aerosol Particle Composition above the Urban Canopy in Beijing: Insights into the
849 Interactions between the Atmospheric Boundary Layer and Aerosol Chemistry, *Environ. Sci. Technol.*, 49(19), 11340–
850 11347, doi:10.1021/acs.est.5b02373, 2015.
- 851 Tang, L., Qu, J. B., Mi, Z. F., Bo, X., Chang, X. Y., Anadon, L. D., Wang, S. Y., Xue, X. D., Li, S. B., Wang, X., and
852 Zhao, X. H.: Substantial emission reductions from Chinese power plants after the introduction of ultra-low emissions
853 standards, *Nat. Energy*, 4, 929–938, <https://doi.org/10.1038/s41560-019-0468-1>, 2019.
- 854 Veld, M. in t., Alastuey, A., Pandolfi, M., Amato, F., Pérez, N., Reche, C., Via, M., Minguillón, M. C., Escudero, M. and
855 Querol, X.: Compositional changes of PM_{2.5} in NE Spain during 2009–2018: A trend analysis of the chemical
856 composition and source apportionment, *Sci. Total Environ.*, 795, doi:10.1016/j.scitotenv.2021.148728, 2021.
- 857 Wang, G., Deng, J., Ma, Z., Hao, J. and Jiang, J.: Characteristics of filterable and condensable particulate matter emitted
858 from two waste incineration power plants in China, *Sci. Total Environ.*, 639, 695–704,
859 doi:10.1016/j.scitotenv.2018.05.105, 2018.
- 860 Wang, G., Deng, J., Zhang, Y., Li, Y., Ma, Z., Hao, J. and Jiang, J.: Evaluating Airborne Condensable Particulate Matter
861 Measurement Methods in Typical Stationary Sources in China, *Environ. Sci. Technol.*, 54(3), 1363–1371,
862 doi:10.1021/acs.est.9b05282, 2020a.
- 863 Wang, K., Yang, L., Li, J., Sheng, Z., He, Q. and Wu, K.: Characteristics of condensable particulate matter before and
864 after wet flue gas desulfurization and wet electrostatic precipitator from ultra-low emission coal-fired power plants in
865 China, *Fuel*, 278(June), 118206, doi:10.1016/j.fuel.2020.118206, 2020b.
- 866 Wang, L. Q., Chen, X., Zhang, Y. B., Li, M. Y., Li, P. F., Jiang, L. H., Xia, Y., Li, Z., Li, J. L., Wang L., Hou, T. Y., Liu
867 W. P., Rosenfeld D., Zhu T., Zhang Y. H., Chen J. M., Wang S. X., Huang Y. L., Seinfeld, J. H., and Yu, S. C.:
868 Switching to electric vehicles can lead to significant reductions of PM_{2.5} and NO₂ across China, *One Earth*, 4, 1037–
869 1048, <https://doi.org/10.1016/j.oneear.2021.06.008>, 2021.
- 870 Wang, L. Q., Li, M. Y., Yu, S. C., Chen, X., Li, Z., Zhang, Y. B., Jiang, L. H., Xia, Y., Li, J. L., Liu W. P., Li, P. F., Eric,
871 L., Rosenfeld, D., and Seinfeld, J. H.: Unexpected rises of ozone in urban and rural areas and sulfur dioxide in rural
872 areas during the coronavirus city lockdown in Hangzhou, China: Implications for air quality, *Environ. Chem. Lett.*,
873 18:1713–1723, doi: 10.1007/s10311-020-01028-3, 2020c.
- 874 Wu, B., Bai, X., Liu, W., Lin, S., Liu, S., Luo, L., Guo, Z., Zhao, S., Lv, Y., Zhu, C., Hao, Y., Liu, Y., Hao, J., Duan, L.
875 and Tian, H.: Non-Negligible Stack Emissions of Noncriteria Air Pollutants from Coal-Fired Power Plants in China:
876 Condensable Particulate Matter and Sulfur Trioxide, *Environ. Sci. Technol.*, 54(11), 6540–6550,
877 doi:10.1021/acs.est.0c00297, 2020.
- 878 Wu, L., Wang, X., Lu, S., Shao, M. and Ling, Z.: Emission inventory of semi-volatile and intermediate-volatility organic
879 compounds and their effects on secondary organic aerosol over the Pearl River Delta region, *Atmos. Chem. Phys.*,
880 19(12), 8141–8161, doi:10.5194/acp-19-8141-2019, 2019.
- 881 Wu, Y., Wang, P., Yu, S., Wang, L., Li, P., Li, Z., Mehmood, K., Liu, W., Wu, J., Lichtfouse, E., Rosenfeld, D. and
882 Seinfeld, J. H.: Residential emissions predicted as a major source of fine particulate matter in winter over the Yangtze
883 River Delta, China, *Environ. Chem. Lett.*, 16(3), 1117–1127, doi:10.1007/S10311-018-0735-6/TABLES/3, 2018.
- 884 Xu, L., Pye, H. O. T., He, J., Chen, Y., Murphy, B. N., and Ng, N. L.: Experimental and model estimates of the
885 contributions from biogenic monoterpenes and sesquiterpenes to secondary organic aerosol in the southeastern United
886 States, *Atmos. Chem. Phys.*, 18, 12613–12637, <https://doi.org/10.5194/acp-18-12613-2018>, 2018.
- 887 Xu, W. Q., Sun, Y. L., Chen, C., Du, W., Han, T. T., Wang, Q. Q., Fu, P. Q., Wang, Z. F., Zhao, X. J., Zhou, L. B., Ji, D.
888 S., Wang, P. C. and Worsnop, D. R.: Aerosol composition, oxidation properties, and sources in Beijing: Results from
889 the 2014 Asia-Pacific Economic Cooperation summit study, *Atmos. Chem. Phys.*, 15(23), 13681–13698,

890 doi:10.5194/acp-15-13681-2015, 2015.

- 891 Yang, F., Li, Z., Liu, H., Feng, P., Tan, H., Zhang, S. and Lu, X.: Emission characteristics of condensable particulate
892 matter and sulfur trioxide from coal-fired power plants, *J. Energy Inst.*, 94, 146–156, doi:10.1016/j.joei.2020.12.003,
893 2021.
- 894 Yang, H. H., Kuei-Ting Lee, Hsieh, Y.-S., Luo, S.-W. and Li, M.-S.: Filterable and Condensable Fine Particulate
895 Emissions from Stationary Sources, *Aerosol Air Qual. Res.*, 14, 2010–2016, doi:10.4209/aaqr.2014.08.0175, 2014.
- 896 Yang, H. H., Arafath, S. M., Lee, K. T., Hsieh, Y. S. and Han, Y. Te: Chemical characteristics of filterable and
897 condensable PM_{2.5} emissions from industrial boilers with five different fuels, *Fuel*, 232(168), 415–422,
898 doi:10.1016/j.fuel.2018.05.080, 2018a.
- 899 Yang, H. H., Arafath, S. M., Wang, Y. F., Wu, J. Y., Lee, K. T. and Hsieh, Y. S.: Comparison of Coal- and Oil-Fired
900 Boilers through the Investigation of Filterable and Condensable PM_{2.5} Sample Analysis, *Energy and Fuels*, 32(3),
901 2993–3002, doi:10.1021/acs.energyfuels.7b03541, 2018b.
- 902 Yu, S., Mathur, R., Pleim, J., Wong, D., Gilliam, R., Alapaty, K., Zhao, C. and Liu, X.: Aerosol indirect effect on the grid-
903 scale clouds in the two-way coupled WRF-CMAQ: Model description, development, evaluation and regional analysis,
904 *Atmos. Chem. Phys.*, 14(20), 11247–11285, doi:10.5194/acp-14-11247-2014, 2014.
- 905 Zhang, Y., Tang, L., Croteau, P. L., Favez, O., Sun, Y., Canagaratna, M. R., Wang, Z., Couvidat, F., Albinet, A., Zhang,
906 H., Sciare, J., Prévôt, A. S. H., Jayne, J. T. and Worsnop, D. R.: Field characterization of the PM_{2.5} Aerosol Chemical
907 Speciation Monitor: Insights into the composition, sources, and processes of fine particles in eastern China, *Atmos.*
908 *Chem. Phys.*, 17(23), 14501–14517, doi:10.5194/acp-17-14501-2017, 2017.
- 909 Zhang, Y., Chen, X., Yu, S., Wang, L., Li, Z., Li, M., Liu, W., Li, P., Rosenfeld, D. and Seinfeld, J. H.: City-level air
910 quality improvement in the Beijing-Tianjin-Hebei region from 2016/17 to 2017/18 heating seasons: Attributions and
911 process analysis, *Environ. Pollut.*, 274, 116523, doi:10.1016/j.envpol.2021.116523, 2021.
- 912 Zhao, B., Wang, S., Donahue, N. M., Jathar, S. H., Huang, X., Wu, W., Hao, J., and Robinson, A. L.: Quantifying the
913 effect of organic aerosol aging and intermediate-volatility emissions on regional-scale aerosol pollution in China, *Sci.*
914 *Rep.*, 6, 28815, <https://doi.org/10.1038/srep28815>, 2016.
- 915 Zhao, B., Wu, W., Wang, S., Xing, J., Chang, X., Liou, K. N., Jiang, J. H., Gu, Y., Jang, C., Fu, J. S., Zhu, Y., Wang, J.,
916 Lin, Y. and Hao, J.: A modeling study of the nonlinear response of fine particles to air pollutant emissions in the
917 Beijing-Tianjin-Hebei region, *Atmos. Chem. Phys.*, 17(19), 12031–12050, doi:10.5194/acp-17-12031-2017, 2017.
- 918 Zhao, Y., Nguyen, N. T., Presto, A. A., Hennigan, C. J., May, A. A. and Robinson, A. L.: Intermediate Volatility Organic
919 Compound Emissions from On-Road Diesel Vehicles: Chemical Composition, Emission Factors, and Estimated
920 Secondary Organic Aerosol Production, *Environ. Sci. Technol.*, 49(19), 11516–11526, doi:10.1021/acs.est.5b02841,
921 2015.
- 922 Zheng, C., Hong, Y., Liu, S., Yang, Z., Chang, Q., Zhang, Y., and Gao, X.: Removal and emission characteristics of
923 condensable particulate matter in an ultralow emission power plant, *Energy & Fuels*, 32(10), 10586-10594,
924 <https://doi.org/10.1021/acs.energyfuels.8b02464>, 2018.
- 925 Zheng, H., Cai, S., Wang, S., Zhao, B., Chang, X. and Hao, J.: Development of a unit-based industrial emission inventory
926 in the Beijing-Tianjin-Hebei region and resulting improvement in air quality modeling, *Atmos. Chem. Phys.*, 19(6),
927 3447–3462, doi:10.5194/acp-19-3447-2019, 2019.
- 928 Zhou, C.: Experimental study on emission and distribution characteristics of organic pollutants in condensable particulate
929 matter in coal-fired flue gas., Master thesis, School of Energy Engineering, Zhejiang University, China, 82 pp., 2019.

937 Table 1 Definitions of some acronyms used in this study.

938

<u>Acronyms</u>	<u>Definitions</u>
<u>FPM</u>	<u>Primary-emitted filterable particulate matter which is in liquid or solid phases in flue</u>
<u>CPM</u>	<u>Primary-emitted condensable particulate matter which is in gas phase at flue gas temperature but condenses or reacts in the ambient air to form solid or liquid PM</u>
<u>OM (CPM)</u>	<u>Organic matter measured in CPM</u>
<u>OM_{si} (CPM)</u>	<u>Organic matter in CPM which is semi-volatile (SVOCs, $10^0 \leq C^* \leq 10^3 \mu\text{g m}^{-3}$), or has intermediate volatility (IVOCs, $10^3 < C^* < 10^6 \mu\text{g m}^{-3}$) are combined as OM_{si} (CPM)</u>
<u>OM ($C^* \leq 100$)</u>	<u>Organic matter with the saturation concentrations (C^*) below $100 \mu\text{g m}^{-3}$</u>
<u>SVOCs</u>	<u>Primary-emitted semi-volatile organic compounds</u>
<u>IVOCs</u>	<u>Primary-emitted intermediate-volatility organic compounds</u>
<u>S/IVOCs</u>	<u>SVOCs + IVOCs</u>
<u>POA</u>	<u>Atmospheric organic aerosol from primary-emitted organic matter or formed by condensation of organic vapors before photochemical reactions</u>
<u>SOA</u>	<u>Atmospheric secondary organic aerosol generated by photochemical reactions and condensation of organic vapors after photochemical reactions</u>
<u>ASOA</u>	<u>SOA generated by photochemical oxidations of anthropogenic volatile organic compounds</u>
<u>BSOA</u>	<u>SOA generated by photochemical oxidations of biogenic volatile organic compounds</u>
<u>SISOA</u>	<u>SOA generated by photochemical oxidations of primary S/IVOCs</u>
<u>OA</u>	<u>POA + SOA</u>

939

940

941

942

943

944

945

946

947

948

949

950

951

952

953

954

955

956

957

958

959

960

961

962

963 Table 24 List of the ratios of the emission rates of OA in condensable particulate matter (CPM)
 964 ($E_{OA}(CPM)$) to those of $PM_{2.5}$ in filterable particulate matter (FPM) ($E_{PM_{2.5}}(FPM)$) from stationary
 965 combustion sources based on the collected references.
 966

method	emission sources	number	$E_{OA}(CPM)/E_{PM_{2.5}}(FPM)$			references
			[Min, Max]	Mean \pm SD	median	
cooling method (EPA 202)	coal-fired power plant	30	[0.01, 25.4]	6.87 ± 7.25	3.99	Li et al. (2017c, 2017d); Li (2018); Li et al. (2019); Lu et al. (2019); Pei (2015); Qi et al. (2017); Song et al. (2020); Wang et al. (2020b); Wu et al. (2020); Yang et al. (2014, 2018b); Yang et al.(2021); Zhou (2019)
	waste incineration power plant	2	[1.64, 4.95]	3.29 ± 1.65	3.29	Wang et al. (2018)
	industrial coal-fired boiler	6	[0.14, 1.03]	0.58 ± 0.34	0.50	Lu et al. (2019) Yang et al. (2014, 2018a, 2018b)
	heavy oil-fired boiler	4	[0.28, 2.49]	1.62 ± 0.88	1.85	Yang et al. (2018a, 2018b)
	wood-fired boiler	1		0.03		
	natural gas-fired boiler	1		6.67		Yang et al. (2018a)
	diesel-fired boiler	1		15.84		
dilution method (ISO 25597)	iron and steel plants	5	[0.32, 7.22]	3.35 ± 2.21	3.00	Yang et al. (2014, 2015)
	incinerator	1		0.12		Yang et al. (2014)
	iron and steel coking plant	1		0.416		Zhang et al. (2020)

967
 968
 969
 970
 971
 972
 973
 974
 975
 976
 977
 978
 979
 980

981 Table 32 Probabilistic distributions with uncertainty ranges in the ratio of $E_{POA}(CPM)$ to $E_{PM2.5}(FPM)$
 982 (95% confidence interval). Para1 represents the mean for normal, and the mean of $\ln(x)$ for lognormal.
 983 Para2 represents the standard deviation for normal, and the standard deviation of $\ln(x)$ for lognormal.
 984 Mean represents the mean for emission ratios of each source category derived from the statistical
 985 bootstrap simulation.
 986

Input parameters	Emission sources	Distribution type	Para1	Para2	Mean	Uncertainty ranges (95% confidence level)
$E_{POA}(CPM)$ $/E_{PM2.5}(FPM)$	Power plant	lognormal	1.07	0.93	4.12	(3.10, 5.29)
	Industry combustion	lognormal	-0.47	1.43	1.38	(0.62, 2.44)
	Steel	normal	2.80	1.98	2.80	(0.92, 4.50)
Total						(-27%, 28%)

987
 988
 989
 990
 991
 992
 993
 994
 995
 996
 997
 998
 999
 1000
 1001
 1002
 1003
 1004
 1005
 1006
 1007
 1008
 1009
 1010
 1011
 1012
 1013
 1014
 1015
 1016
 1017
 1018
 1019

Table 43 Simulation case design. PP, IN, IR, and TR denote source sectors of power plant, industry combustion, steel, and transportation, respectively. Three kinds of scaling factors for the five volatility bins of organic CPM are tested: fac1 (0, 0.18, 0.14, 0.18, 0.5), fac2 (0, 0.66, 0.40, 0.51, 1.43), and fac3 (0, 0.42, 0.27, 0.345, 0.965) which is the average of fac1 and fac2. ~~fac1 (0.09, 0.09, 0.14, 0.18, 0.5) (Grieshop et al., 2009), fac2 (0.40, 0.26, 0.40, 0.51, 1.43) (Shrivastava et al., 2011), and fac3 (0.245, 0.175, 0.27, 0.345, 0.965) which is the average of fac1 and fac2.~~

Simulation Cases	Aerosol module	$E_{PP_POA}(CPM)$ $/E_{PM2.5}(FPM)$	$E_{IN_POA}(CPM)$ $/E_{PM2.5}(FPM)$	$E_{IR_POA}(CPM)$ $/E_{PM2.5}(FPM)$	Volatility bins
Only	AERO6VBS	0	0	0	
FPM	AERO7_def	0	0	0	
	AERO7_adj	0	0	0	
S1.1	AERO7	4.12	1.38	2.80	fac1
S1.2	AERO7	4.12	1.38	2.80	fac2
S1.3	AERO7	4.12	1.38	2.80	fac3
S2.1	AERO7	3.01	1.01	2.04	fac1
S2.2	AERO7	3.01	1.01	2.04	fac2
S3.1	AERO7	5.27	1.77	3.58	fac1
S3.2	AERO7	5.27	1.77	3.58	fac2
S4.2	AERO7	3.71	1.24	2.52	fac2
S5.2	AERO7	4.49	1.50	3.05	fac2
S6_TR	AERO7	0	0	0	fac1
S7_IN	AERO7	0	1.38	0	fac1
S8_IR	AERO7	0	0	2.80	fac1
S9_PP	AERO7	4.12	0	0	fac1

Simulation Cases	Aerosol module	$E_{PP_OM}(CPM)$ $/E_{PM2.5}(FPM)$	$E_{IN_OM}(CPM)$ $/E_{PM2.5}(FPM)$	$E_{IR_OM}(CPM)$ $/E_{PM2.5}(FPM)$	Volatility bins
Only	AERO6VBS	0	0	0	
FPM	AERO7	0	0	0	
S1.1	AERO7	4.12	1.38	2.80	fac1
S1.2	AERO7	4.12	1.38	2.80	fac2
S1.3	AERO7	4.12	1.38	2.80	fac3
S2.1	AERO7	3.01	1.01	2.04	fac1
S2.2	AERO7	3.01	1.01	2.04	fac2
S3.1	AERO7	5.27	1.77	3.58	fac1
S3.2	AERO7	5.27	1.77	3.58	fac2
S4.2	AERO7	3.71	1.24	2.52	fac2
S5.2	AERO7	4.49	1.50	3.05	fac2
S6_TR	AERO7	0	0	0	fac1
S7_IN	AERO7	0	1.38	0	fac1
S8_IR	AERO7	0	0	2.80	fac1
S9_PP	AERO7	4.12	0	0	fac1

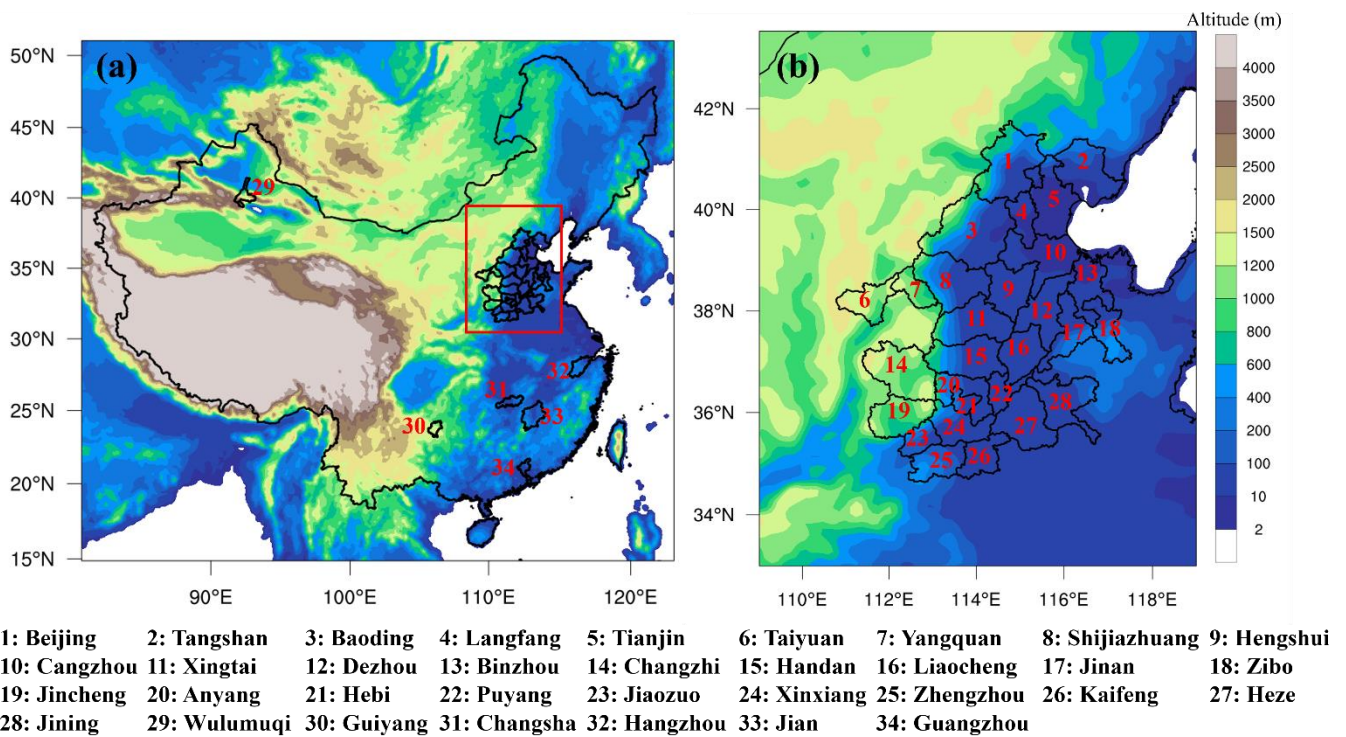
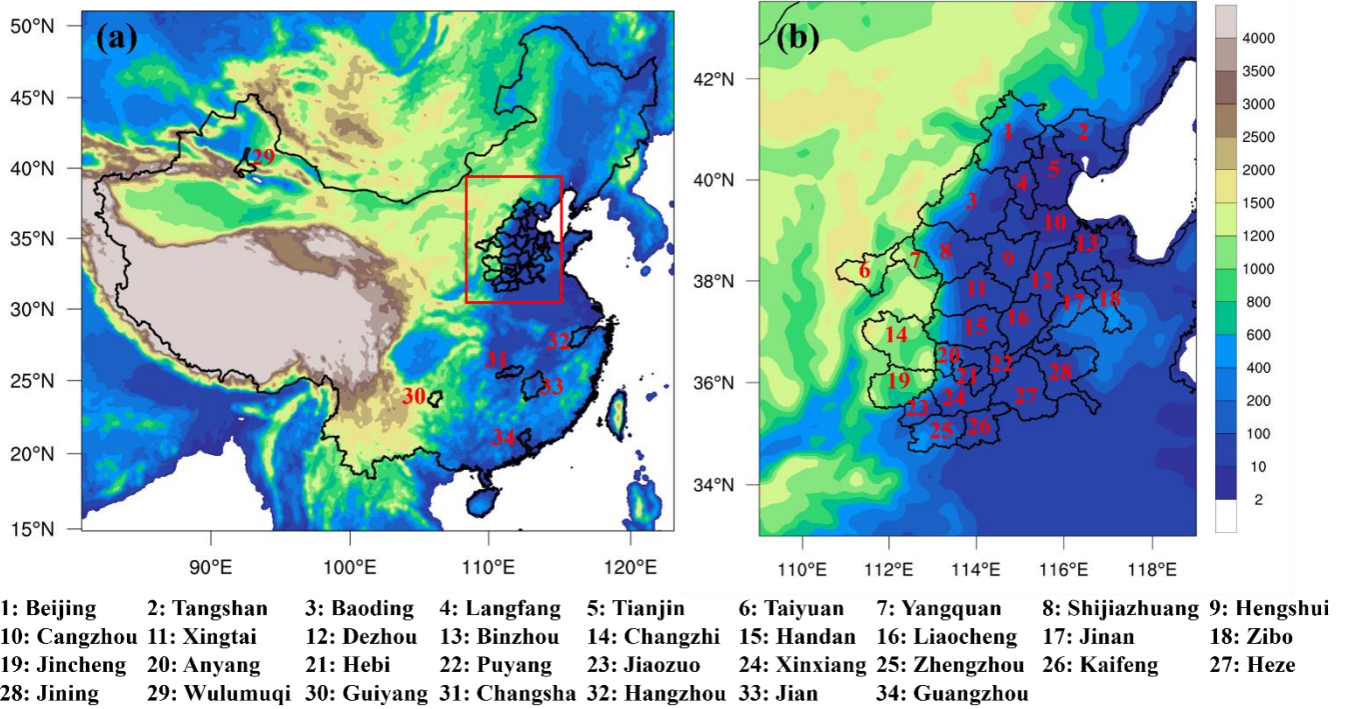
1031
1032
1033
1034

Table 4-5 Model evaluation statistics for hourly OA, POA and SOA concentrations during October 14–November 14, 2014, and daily OA concentrations during December 6–30, 2018, under different sensitivity simulation cases.

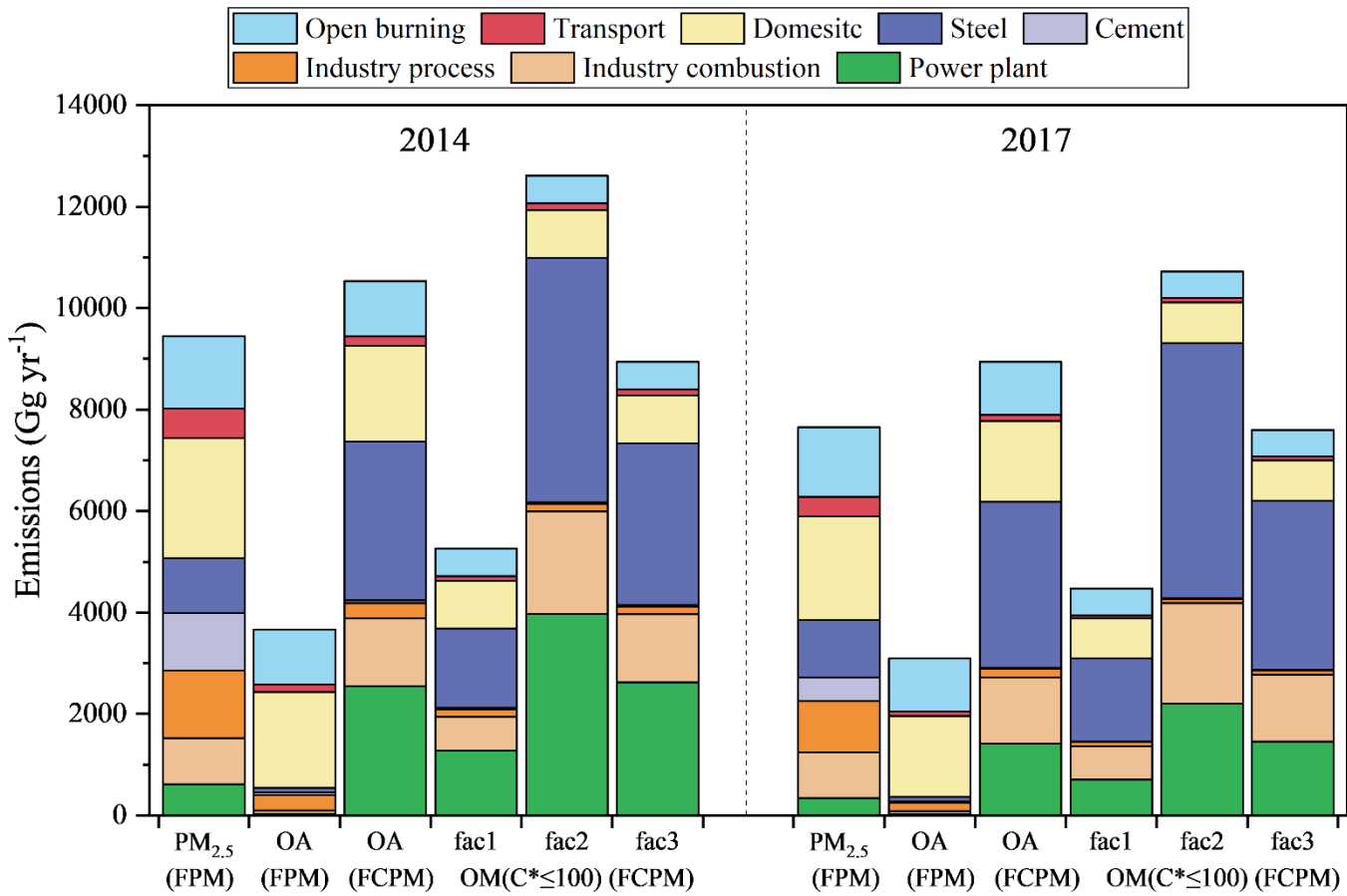
Period	City	Species	Cases	N	OBS	SIM	MB	NMB	NME	R
October 14– November 14, 2014	Beijing	OA	base	723	33.71	11.90	-21.81	-64.70%	64.84%	0.71
			S1.1		33.71	25.08	-8.63	-25.60%	47.00%	0.70
			S1.2		33.71	39.38	5.67	16.82%	58.62%	0.69
			S1.3		33.71	31.88	-1.83	-5.43%	49.63%	0.70
		POA	base	723	16.25	4.28	-11.97	-73.66%	73.75%	0.54
			S1.1		16.25	10.24	-6.01	-36.98%	54.01%	0.54
			S1.2		16.25	23.32	7.07	43.51%	87.16%	0.53
			S1.3		16.25	16.45	0.20	1.23%	61.57%	0.53
		SOA	base	723	17.46	7.62	-9.84	-56.36%	57.22%	0.74
			S1.1		17.46	14.85	-2.61	-14.95%	47.42%	0.73
			S1.2		17.46	16.05	-1.41	-8.08%	48.24%	0.73
			S1.3		17.46	15.42	-2.04	-11.68%	47.75%	0.73
December 6–30, 2018	Handan	OA	base	25	45.24	17.70	-27.54	-60.88%	60.89%	0.62
			S1.1		45.24	35.04	-10.20	-22.55%	38.00%	0.61
			S1.3		45.24	48.86	3.62	8.00%	38.95%	0.59
	Shijiazhuang	OA	base	25	42.22	18.38	-23.84	-56.47%	57.45%	0.61
			S1.1		42.22	38.88	-3.34	-7.91%	35.69%	0.61
			S1.3		42.22	58.02	15.80	37.42%	47.27%	0.61
	Xingtai	OA	base	25	42.22	13.35	-28.87	-68.38%	68.37%	0.58
			S1.1		42.22	29.34	-12.88	-30.51%	40.59%	0.58
			S1.3		42.22	42.56	0.34	0.81%	34.52%	0.56
	Dezhou	OA	base	23	41.66	15.48	-26.18	-62.84%	63.49%	0.47
			S1.1		41.66	31.25	-10.41	-24.99%	42.76%	0.54
			S1.3		41.66	42.58	0.92	2.21%	43.06%	0.56

1035
1036
1037

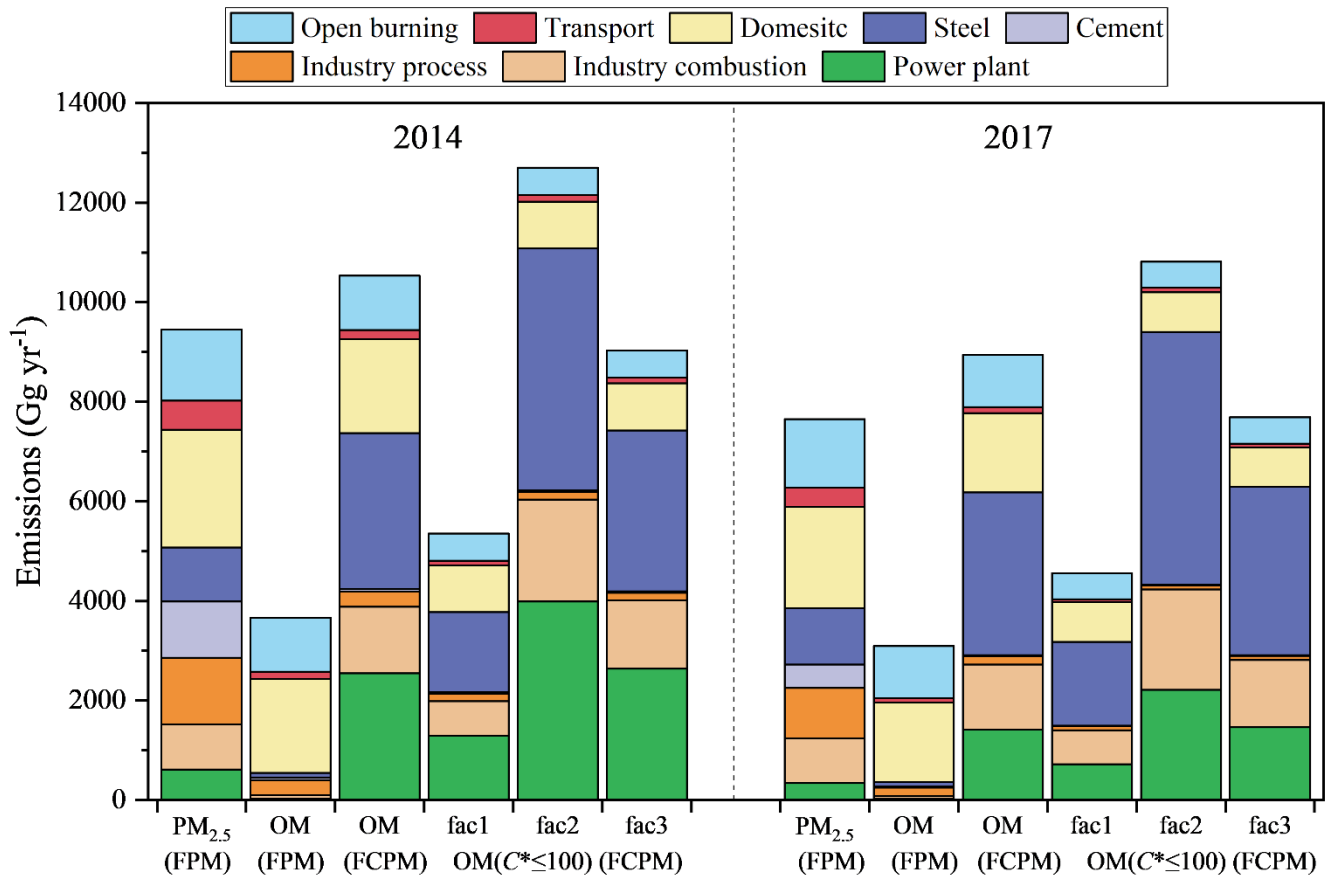
Note: OBS and SIM denote mean concentrations ($\mu\text{g m}^{-3}$) of observations and simulations, respectively; MB: mean bias; NMB: normalized mean bias; NME: normalized mean error; R: correlation coefficient.



1049



1050

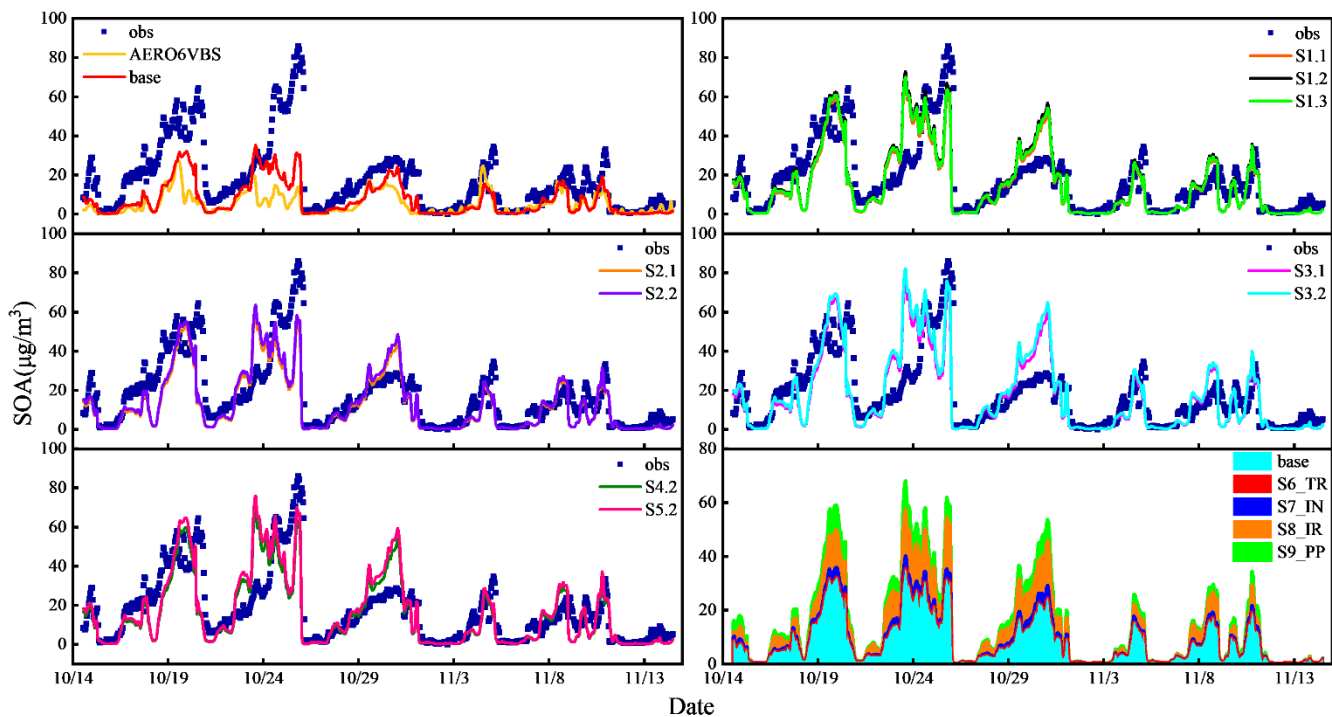


1051

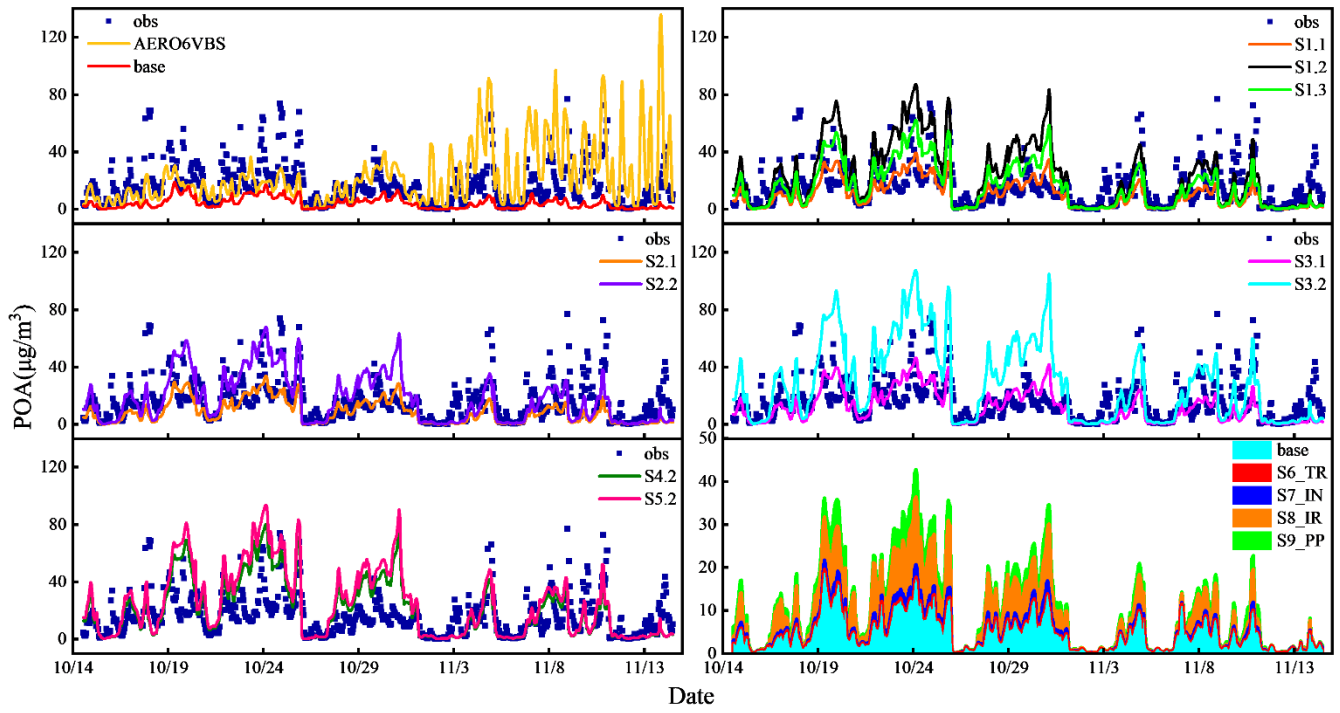
1052

Figure 2. Annual emissions of PM_{2.5} and OA in filterable particulate matter (FPM), OA in filterable plus

1053 condensable particulate matter (FCPM) before the volatility distributions, and OM ($C^* \leq 100$) in FCPM
 1054 after application of the volatility distributions for the fac1, fac2 and fac3 cases over China in 2014 and
 1055 2017.
 1056
 1057
 1058
 1059



1060
 1061 Figure 3. The observed and simulated hourly SOA concentrations during the episode from October 14 to
 1062 November 14, 2014 at the Beijing site in the sensitivity cases as summarized in Table 3.
 1063
 1064
 1065
 1066
 1067
 1068
 1069
 1070
 1071
 1072
 1073
 1074
 1075
 1076
 1077
 1078
 1079
 1080
 1081



1082

1083

1084

1085

1086

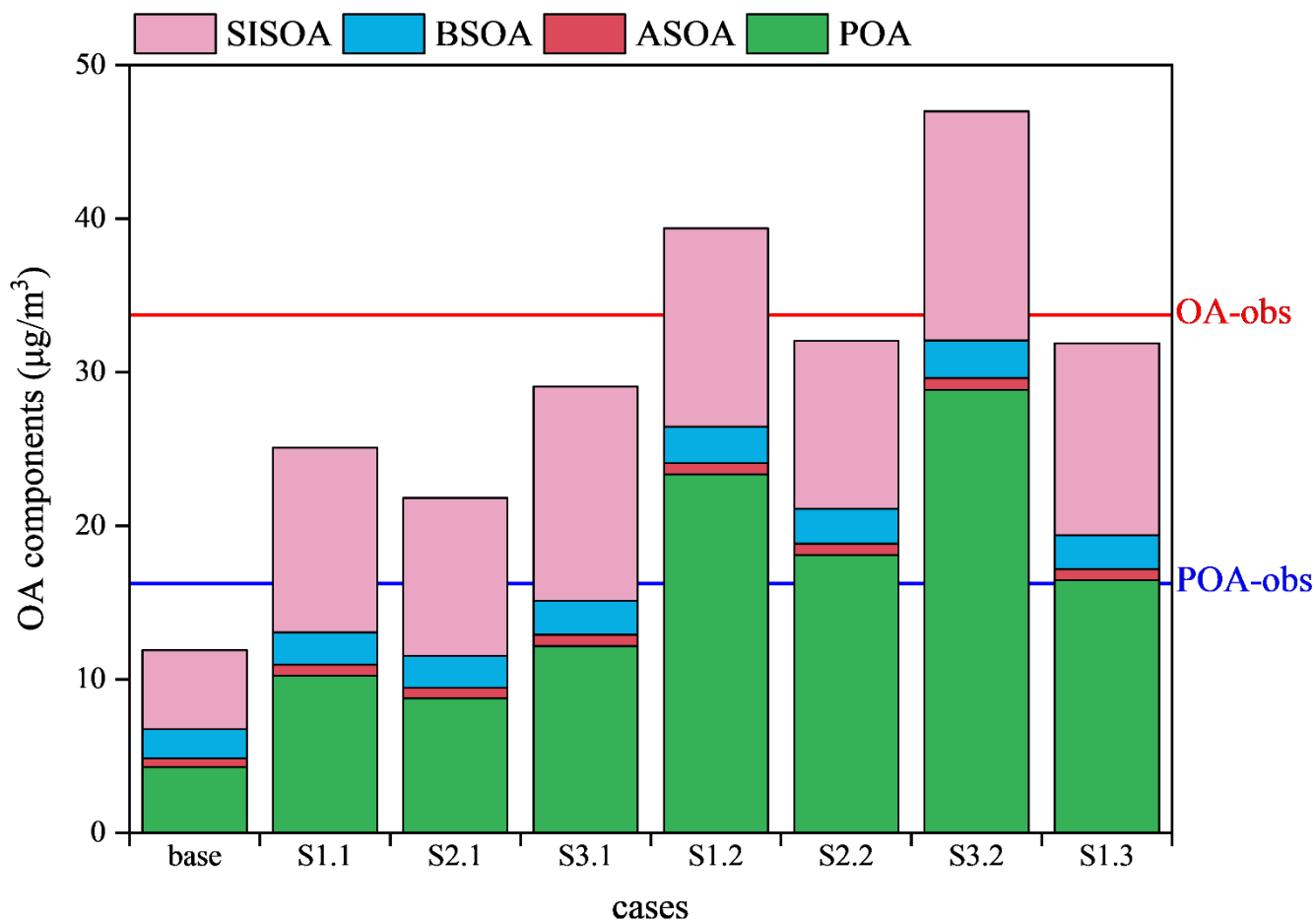
1087

1088

1089

1090

Figure 4. The observed and simulated hourly POA concentrations during the episode from October 14 to November 14, 2014 at the Beijing site in the sensitivity cases as summarized in Table 3.



1091
 1092 Figure 5. The simulation concentrations of different OA components averaged over the whole study
 1093 period from October 14 to November 14, 2014 at the Beijing site in the sensitivity cases. AERO7_def is
 1094 abbreviated as def and AERO7_adj as adj. ASOA, BSOA and SISOA denote SOA generated by
 1095 anthropogenic VOCs, biogenic VOCs and low volatile S/IVOCs, respectively. The red and blue horizontal
 1096 line denote the average observation concentrations of OA and POA, respectively.
 1097
 1098
 1099
 1100

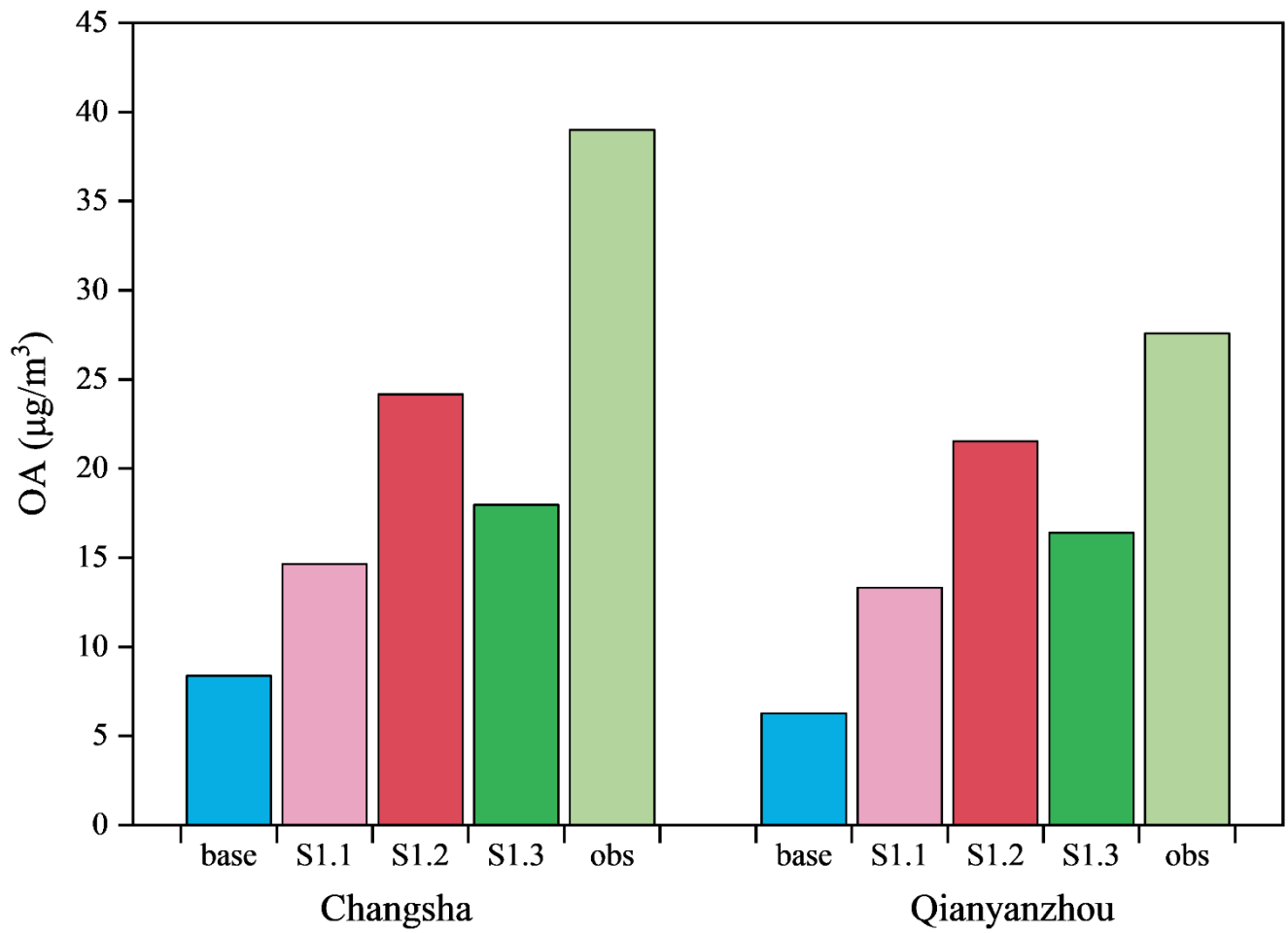
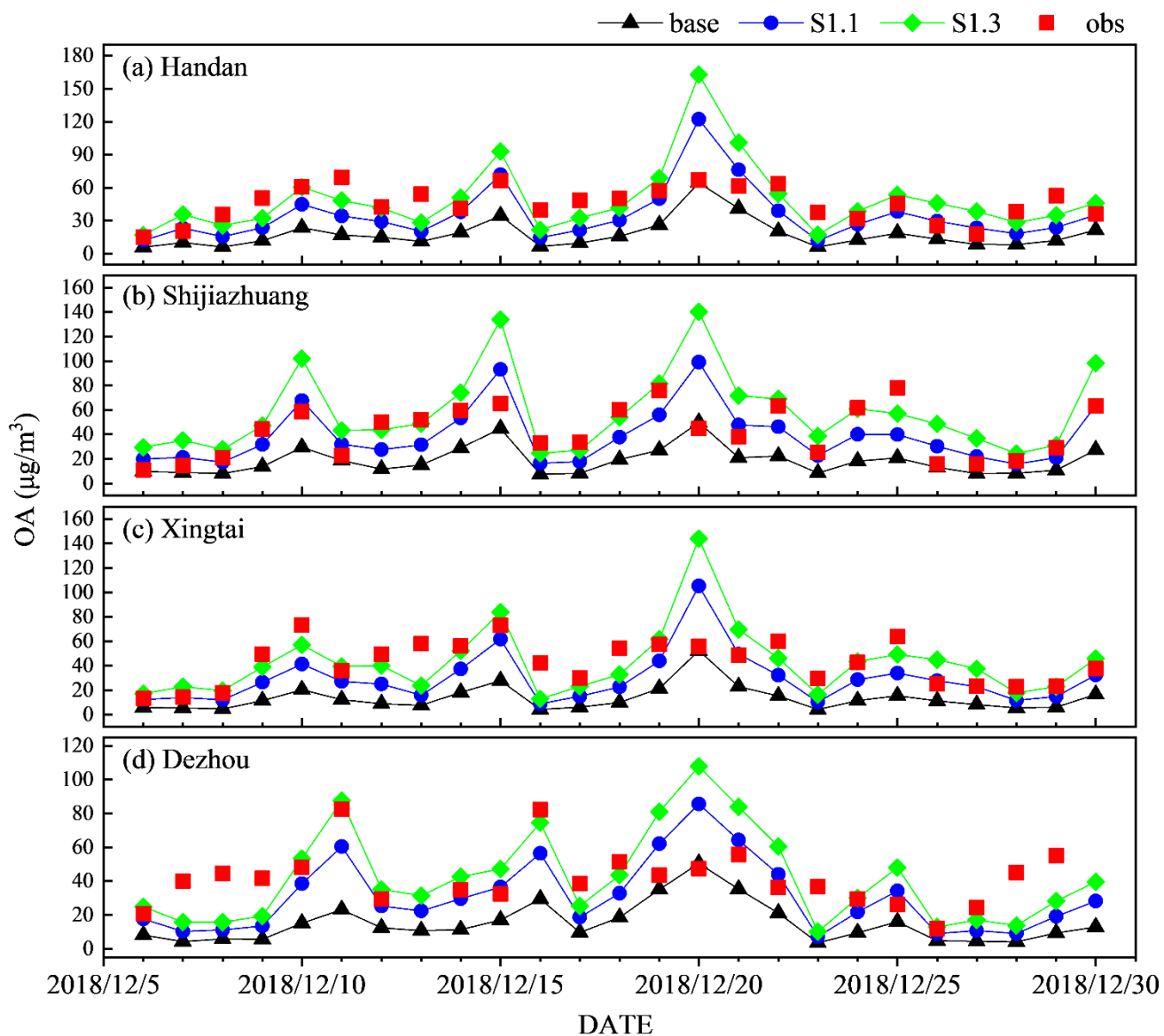


Figure 6. The observed and simulated OA concentrations in the sensitivity cases on November 3, 2014 at Changsha and Qianyanzhou.

1101
 1102
 1103
 1104
 1105
 1106
 1107
 1108
 1109
 1110
 1111
 1112
 1113
 1114
 1115
 1116
 1117



1118

1119 Figure 7. The observed and simulated daily OA concentrations during December 6-30 in 2018 at (a)
 1120 Handan, (b) Shijiazhuang, (c) Xingtai and (d) Dezhou.

1121

1122

1123

1124

1125

1126

1127

1128

1129

1130

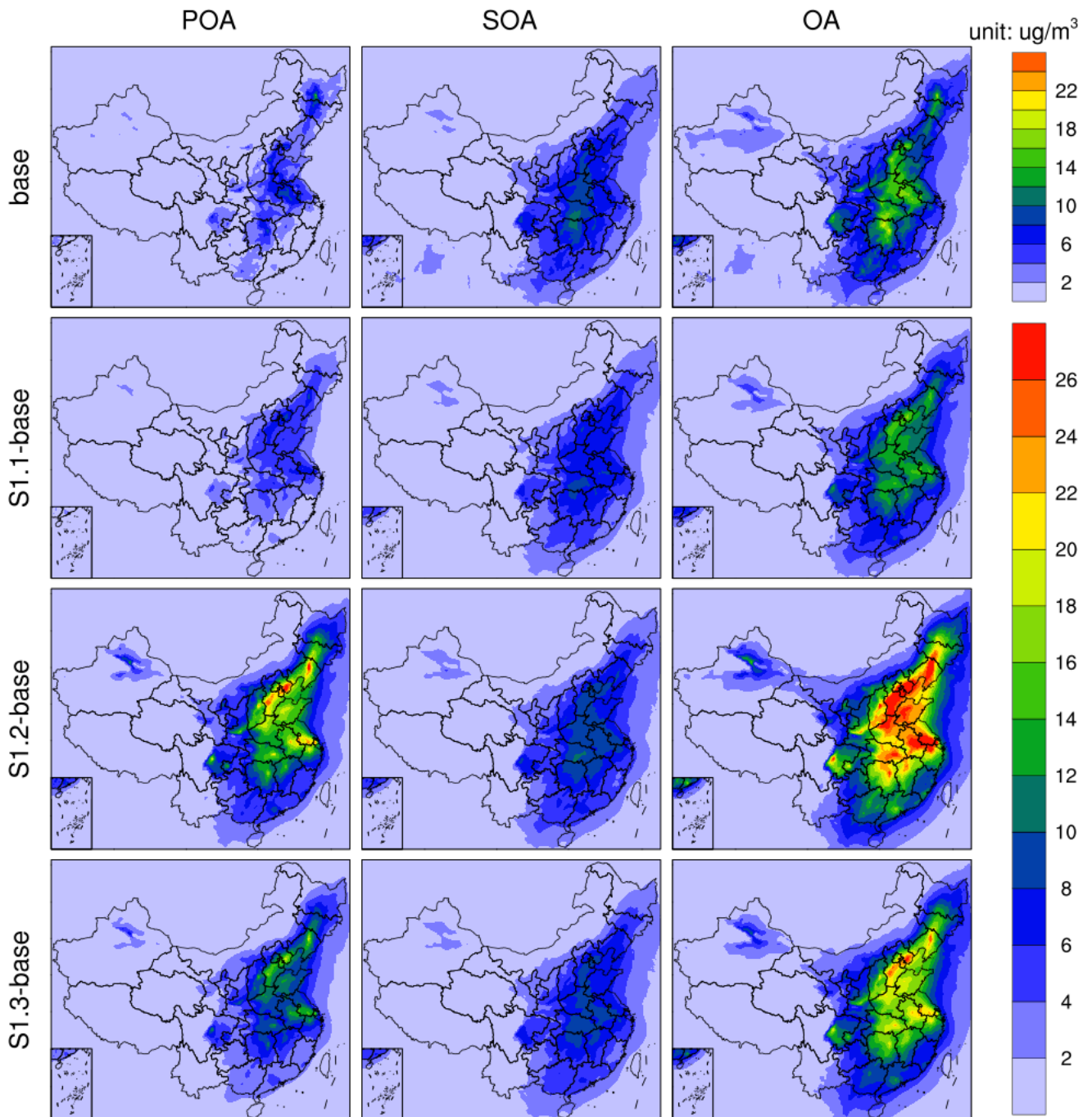
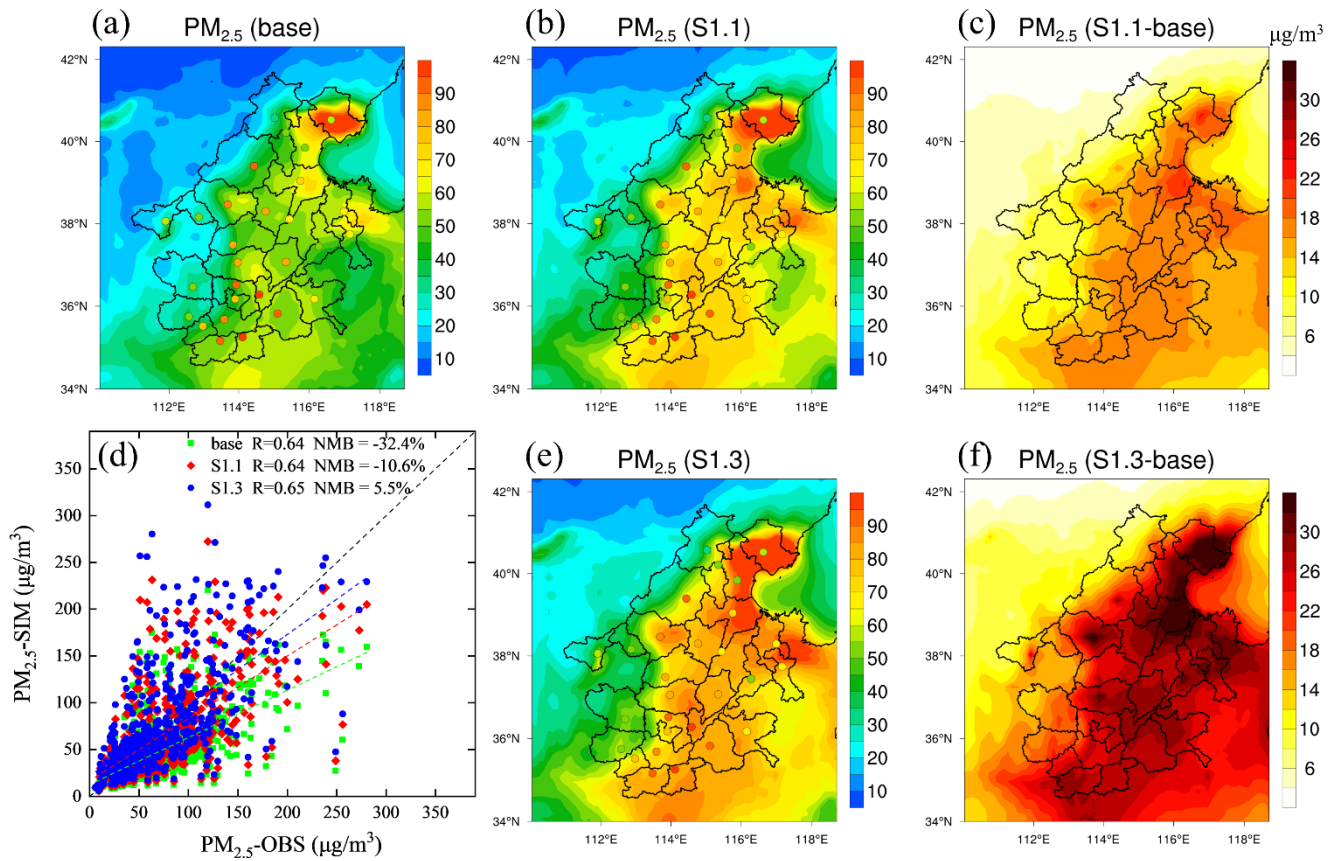


Figure 8. Spatial distributions of the concentrations of POA, SOA and OA averaged over the whole period of October 14–November 14 in 2014 generated by the simulations with FPM sources (base) and CPM sources (S1.1-base, S1.2-base, S1.3-base).

1131
 1132
 1133
 1134
 1135
 1136
 1137
 1138
 1139
 1140
 1141



1142

1143 Figure 9. Spatial distributions of the average $PM_{2.5}$ concentrations during December 6-30, 2018, over the
 1144 BTH2+26 cities in (a) base, (b) S1.1, (e) S1.3, (c) absolute difference between S1.1 and base, and (f)
 1145 absolute difference between S1.3 and base. Among them, the $PM_{2.5}$ concentrations from December 22 to
 1146 26 are not included due to the missing observation data. (d) Scatter plots and linear regressions of
 1147 observed (OBS) and simulated (SIM) daily $PM_{2.5}$ concentrations for all of the BTH2+26 cities during the
 1148 above time period under the base, S1.1, and S1.3 scenarios.

1149

1150

1151

1152

1153

1154

1155

1156

1157

1158

1159

1160

1161

1162

1163

1164

1165

1166

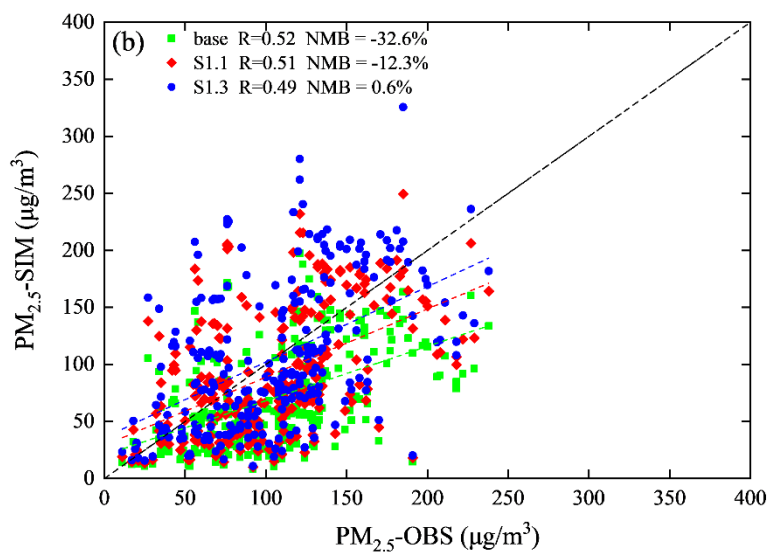
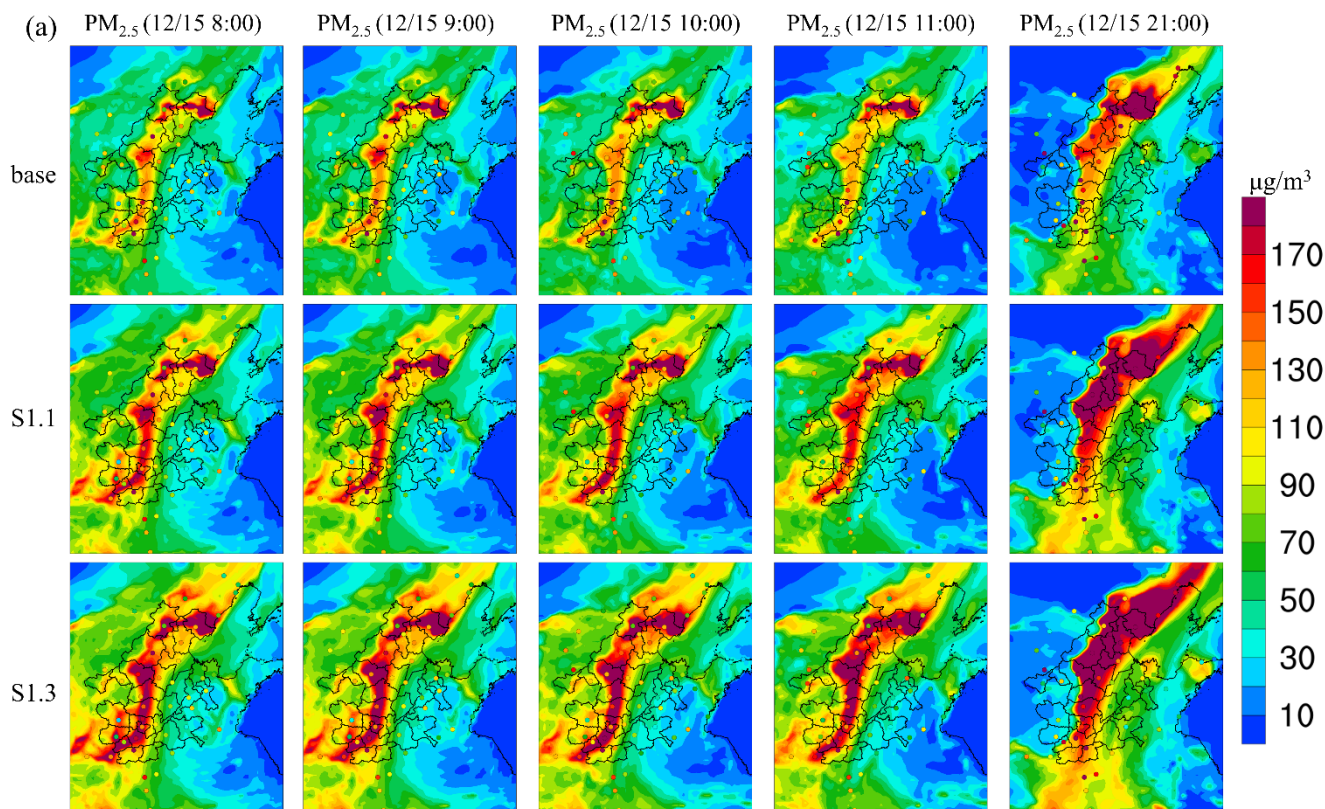


Figure 10. (a) Spatial distributions of hourly $PM_{2.5}$ concentrations at some peak hours over the BTH2+26 cities under the base, S1.1, and S1.3 scenarios. The colored dots denote observation values for each city. (b) Scatter plots and linear regressions of observed (OBS) and simulated (SIM) hourly $PM_{2.5}$ concentrations for all cities under the base, S1.1, and S1.3 scenarios.